ERDC/ITL TR-15-1

Information Technology Laboratory

US Army Corps of Engineers®
Engineer Research and Development Center

ERDC
INNOVATIVE SOLUTIONS for a safer, better world

Detection of Microcracks in Trunnion Rods Using Ultrasonic Guided Waves

James A. Evans and Richard W. Haskins

July 2015

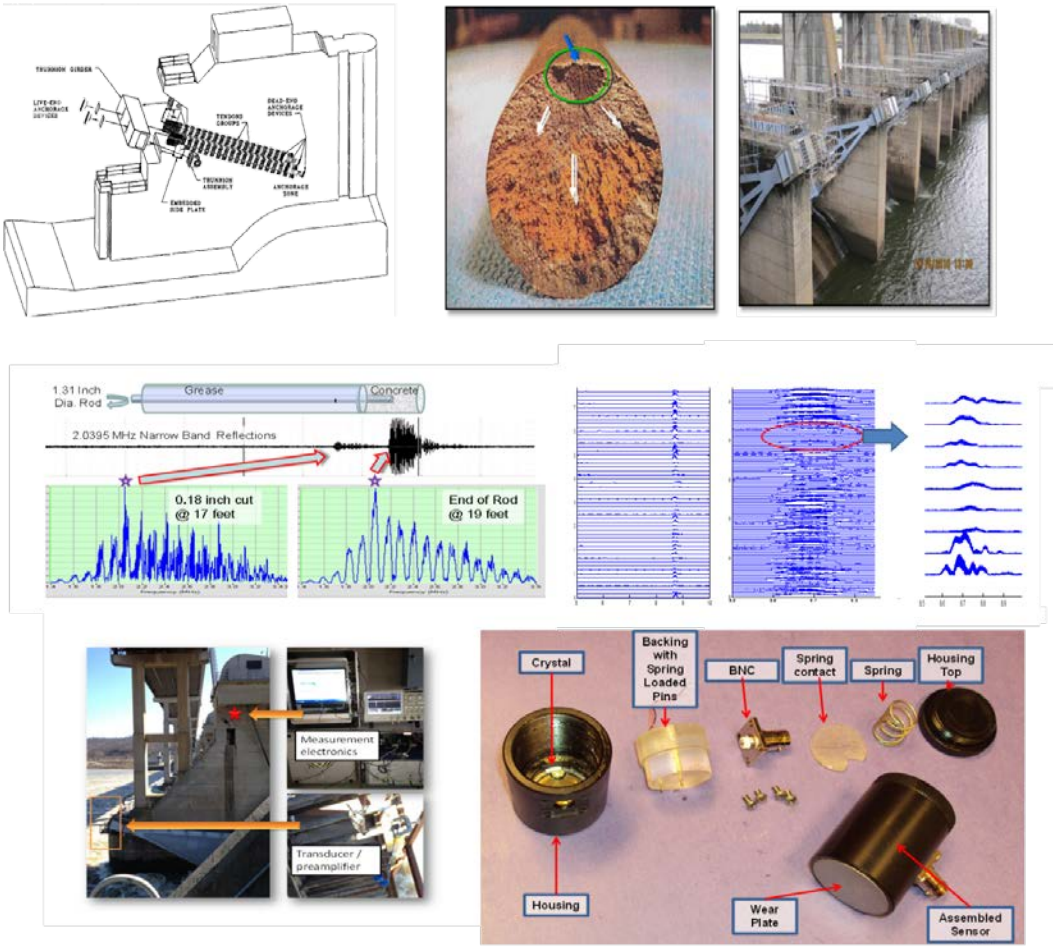

The US Army Engineer Research and Development Center (ERDC) solves the nation's toughest engineering and environmental challenges. ERDC develops innovative solutions in civil and military engineering, geospatial sciences, water resources, and environmental sciences for the Army, the Department of Defense, civilian agencies, and our nation's public good. Find out more at www.erdc.usace.army.mil.

To search for other technical reports published by ERDC, visit the ERDC online library at http://acwc.sdp.sirsi.net/client/default.

ERDC/ITL TR-15-1
July 2015

Detection of Microcracks in Trunnion Rods Using Ultrasonic Guided Waves

James A. Evans and Richard W. Haskins

Information Technology Laboratory
U.S. Army Engineer Research and Development Center
3909 Halls Ferry Road
Vicksburg, MS 39180-6199

Final report

Prepared for U.S. Army Corps of Engineers
Washington, DC 20314-1000

Abstract

Posttensioned rods are used to anchor spillway gates and transfer the forces from the reservoir pool through the gates to the spillway structures. Large tensile loads are applied to these high-strength steel rods to compress the surrounding concrete and prevent it from experiencing excessive destructive tensile forces. These rods are now experiencing ongoing failures. The U.S. Army Corps of Engineers is in need of reliable nondestructive testing (NDT) methods that are rapid, robust, and capable of detecting and quantifying defects.

Methods to detect microcracks are required to be rapid because of the large number of rods that exist at some installations. Robustness is required to handle the significant variations in design, construction, and field conditions that are known to exist. Defect detection and quantification provide tracking and monitoring data important for planning and prioritizing remediation efforts or operational practices.

This research to date has defined and demonstrated acoustical guided waves as a methodology to detect cracks that are orthogonal to the axis of the trunnion rods. A test method and equipment specifications have been developed as well as methods for dealing with field conditions such as anchor rods with rough-cut ends.

Contents

Abstract ii

Figures and Tables v

Preface vii

Unit Conversion Factors viii

1 Introduction 1

1.1 Background 1
1.2 Purpose of work unit 2
1.3 Field conditions 4
1.4 Existing technologies for defect detection 5

2 NDT System Development 7

2.1 Test bed 7
2.2 Guided-wave methods 7
2.2.1 Rod waves 10
2.2.2 Higher-order longitudinal modes 11
2.2.3 Physical propagation influences 14
2.2.4 Nonlinear investigations 15
2.3 Greenup Lock and Dam field testing 15
2.3.1 Tension testing 16
2.3.2 Guided-wave tension influence 17
2.3.3 Pre-Greenup Lock and Dam ERDC test-bed investigations 18
2.3.4 Guided-wave testing at Greenup Lock and Dam 20
2.3.5 Post-Greenup Lock and Dam system optimization 24
2.3.6 Results and conclusions from the Greenup Lock and Dam effort 27

3 NDT System Operation and Components 29

3.1 Test method of current system 29
3.2 Embedded system requirements 29
3.3 Optimization of system 30

4 Rod Coupling 33

4.1 Saw cutting of rod ends 34
4.2 Grinding 35
4.3 Coupling to rough surfaces 36
4.3.1 Description of an ideal couplant 37
4.3.2 Low melting point metals for ultrasonic coupling 37
4.3.3 Field's metal 38
4.3.4 Field's metal coupling as a function of surface condition 40
4.3.5 Guided-wave spectrum and surface condition 43

4.3.6 Recommendations for Field's metal-based coupling 44
4.4 Proof of concept for automated end finishing 45

5 PMN-PT Transducers 48

6 Conclusions and Recommendations 51

References 52

Appendix A: Nonlinear Investigations 55

Report Documentation Page

Figures and Tables

Figures

Figure 1. Cracked trunnion rod from R.F. Henry Lock and Dam. 1
Figure 2. Utilization of anchor rod NDT. 3
Figure 3. Typical exposed end of trunnion anchor rod (side view) in 3a. Figure 3b displays a schematic of trunnion rod anchorage from EM 1110-2-2702 (Figure 5-1) (HQUSACE 2000). 5
Figure 4. Full-scale 4-rod test bed during construction and concrete placement. 7
Figure 5. Acoustical pulse echo from the end of the trunnion anchor rod. 8
Figure 6. Torsional and longitudinal reflections from a shallow, 9 mm saw cut. 10
Figure 7. Narrowband tuning removes echoes from clamp, which simulates steel-on-steel contact. 11
Figure 8. Low-loss modes existing between centralization of guided-wave energy at higher frequency and lower material attenuation at lower frequencies. 13
Figure 9. Energy velocity curves showing compression and torsional modes (left). Reverberation of high–frequency, low-loss modes and the associated A-scan (right). 13
Figure 10. Narrow-band spectral reflections at a 0.18 in. deep cut and the rod end of a 1.31 in. diameter grease-embedded trunnion anchor rod with concrete termination. 14
Figure 11. Variation in load and the resulting influence on propagation delay. 21
Figure 12. Location of testing equipment at Greenup Lock and Dam. 21
Figure 13. Three frequency scans at Greenup Lock and Dam and the selected low-loss inspection mode. 22
Figure 14. Typical signals showing front-end information loss due to high gain required for echo detection (right is zoomed in with overlaid receiver's phase-detected signal shown in green and radio frequency (RF) pulse shown in blue). 23
Figure 15. Various representations of some of the Greenup Lock and Dam test data. The *x*-axis is time in milliseconds (msec). 24
Figure 16. Shift in ideal inspection frequency as observed for a group of rods (pier 2, east bank). 25
Figure 17. Improvement from Accuscan transducer over dual element used at Greenup Lock and Dam. 26
Figure18. Top signal shows Greenup Lock and Dam setting and front-end saturation for the representative small laboratory rod; the bottom signal shows the improvement after TCG application. 27
Figure 19. Block diagram of optimized system configuration. 27
Figure 20. Migration of system from laboratory equipment to portable system. 31
Figure 21. Torch-cut rod ends. 33
Figure 22. A portable band saw used to cut ends of rods. 34
Figure 23. Angle grinder disc producing best results for rod finishing. 35
Figure 24. Waveforms of Fields metal through-transmissions. 39
Figure 25. Casting fixture. 39

Figure 26. Rod end castings. 40
Figure 27. Flat Field's metal coupling piece amplitude of first two echoes used to estimate coupling efficiency. 41
Figure 28. Medium and rough surface Field's metal castings. 41
Figure 29. Field's metal coupling performance to various surface conditions (dB). 42
Figure 30. Field's metal coupling performance to various surface conditions in percentages. 42
Figure 31. Long-distance propagation verified through flat ingot of Field's metal. 43
Figure 32. Spectral frequency shift as surface roughness increases. 44
Figure 33. Through-hole chuck that would serve as a rod-mounted platform for finishing. 45
Figure 34. Side view and end view of cone grinding process for end-of-rod finishing. 46
Figure 35. Example grinding cups (left); cup and rod prior to grinding (right). 46
Figure 36. Second-pass grinding (left); finished surface (center); resulting flatness (right) 47
Figure 37. Components in PMN-PT transducer with interchangeable backing material. 48
Figure 38. Guided-wave rod scan with PMN-PT showing limited bandwidth. 49
Figure 39. Second and third reflections on embedded rod from PMN-PT transducer. 49
Figure 40. Larger second echo from PMN-PT vs. PZT transducer. 50
Figure. 41 Nonlinear crack simulations: two polished ends pulled together (top left), fatigued aluminum (bottom left), nut coupled and shims hammered into a notch (right). 57
Figure 42. Nonlinear modulation detected using torsional wave and impact modulation. 58
Figure 43. The principles of the IIM method. 59
Figure 44. The principles of the IIM method for the same-side excitation. 60
Figure 45. Schema of the experimental setup for measurements of the interaction of the HF tone burst signal with impact-produced acoustic impulse. 61
Figure 46. The contact between two rods imitating the crack. 61
Figure 47. The example of the recorded signal when the sequence of the mechanical pulses (red) and the HF pulses (blue) is presented in the plot above. 63
Figure 48. The LF mechanical impulse recorded by sensor near the crack (red) and the HF pulse at the same point (blue) for the time delay τ= 0.54 msec. 64
Figure 49. The LF mechanical impulse recorded by the Panametrics sensor (red) and the HF pulse reflected from the simulated crack (blue) for the time delay τ= 0.54 msec. 64
Figure 50. The LF mechanical impulse recorded by the Panametrics sensor (red) and the HF pulse reflected from the simulated crack (blue) for the time delay τ =1.4 ms. There is no interaction between these pulses. 65

Tables

Table 1. Low attenuation modes for various rod diameters. 19
Table 2. Assemblies contained in present system. 31
Table 3. Typical couplant materials acoustic characteristics. 37
Table 4. Rod lengths in feet that can be inspected as a function of surface roughness. 43

Preface

This technical report describes the results of the research effort to develop a method to assess the condition of trunnion rods in U.S. Army Corps of Engineer (USACE) dams.

The investigation reported herein was authorized by Headquarters, USACE (HQ USACE), and was performed from Oct 2011 to September 2014 under the Navigation Systems Research Program, Work Unit 70F138, Detection of Microcracks in Trunnion Rods Using Non-Linear Acoustics. Jeff McKee was the HQUSACE Business Line Manager.

The Program Manager for the Navigation Systems Research Program was Charles Wiggins, Coastal and Hydraulics Laboratory (CHL), U.S. Army Engineer Research and Development Center (ERDC). W. Jeff Lillycrop was the Technical Director for Navigation, CHL. The investigation was led by James Evans, Information Technology Laboratory (ITL), who was Principal Investigator of Work Unit 70F138.

This report was authored by James Evans and Richard W. Haskins, both of the Sensor Measurement and Instrumentation Branch (SMIB), ITL.

At the time this research was conducted at ITL, Dr. Reed L. Mosher was Director, Patti Duett was Deputy Director, and Dr. Robert M. Wallace was Chief, Computational Science and Engineering Division (CSED). At CHL, Dr. William D. Martin was Director, José E. Sánchez was Deputy Director, and Dr. Rose Kress was Chief, Navigation Division.

Special thanks is given to Dr. Robert Moser, Geotechnical and Structures Laboratory (GSL), for his collaborative efforts provided on this project, Ken Switzer for his continuous help on construction of various aspects of the project, and Dan Wilson (GSL) for his help on the equipment.

Appreciation is also given to project collaborators Cody Borigo of Feature Based Systems (FBS) and Dr. Joseph Rose of both Penn State University and FBS and also Dr. Alexander Sutin of the Stevens Institute of Technology.

At the time of publication LTC John T. Tucker III was the Acting Commander, ERDC, and Dr. Jeffery P. Holland was Director.

Unit Conversion Factors

Multiply	By	To Obtain
degrees Fahrenheit	(F-32)/1.8	degrees Celsius
feet	0.3048	meters

1 Introduction

Catastrophic failure of posttensioned trunnion anchor rods at dams is an ongoing problem caused by propagating orthogonal cracks. The source of this cracking is believed to be due to stress corrosion cracking and possibly hydrogen embitterment. The condition is shown in Figure 1 and presents a rod that had failed and was removed from R.F. Henry Lock and Dam.

Figure 1. Cracked trunnion rod from R.F. Henry Lock and Dam.

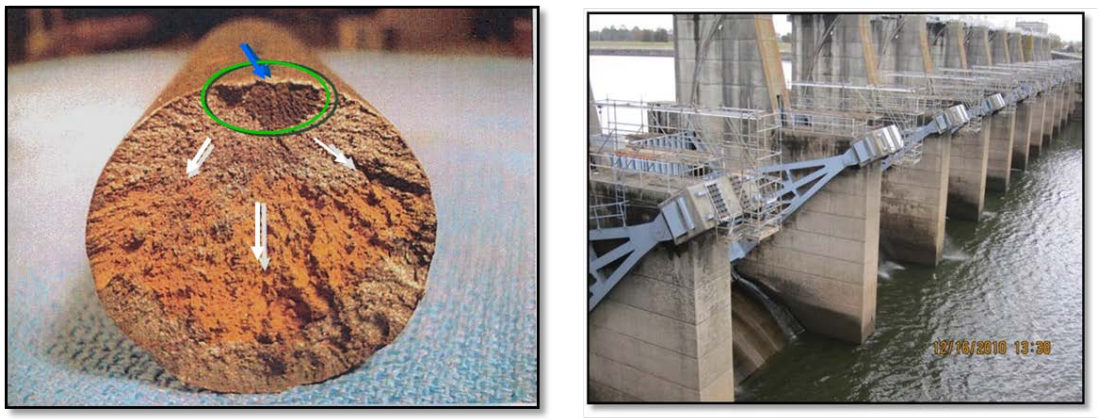

The dam has 376 trunnion rods supporting the tainter gates. In the broken-rod image (Figure 1), a blue arrow has been drawn to indicate the fracture origin with white arrows drawn to indicate the crack propagating direction. The green ellipse encircles an area that appears to have been a pre-existing crack, which is more heavily oxidized than the rest of the fracture surface. The focus of this research is to develop a nondestructive test method capable of detecting the prefailure condition of the rod when the crack area is smaller than the green elipse shown in Figure 1. The right side of Figure 1 shows the tainter gate trunnion rods located on a dam pier. The function of the trunnion anchor rods is to posttension the structure in order to prevent excessive tensile loading of the concrete.

1.1 Background

Posttensioned rods are used to anchor spillway gates and transfer the forces from the reservoir pool through the gates to the spillway structures. Large tensile loads are applied to these high-strength steel rods to compress the surrounding concrete and prevent it from experiencing excessive tensile forces, which are naturally problematic for concrete. The Headquarters,

U.S. Army Corps of Engineers (HQ USACE) specification in Engineer Manual (EM) 1110-2-2702 (HQ USACE 2000), requires the use of posttensioned trunnion anchor rods in the design of spillway tainter gates in the 1960s and constructed several navigation, flood control, and hydro-electric projects during the 1960s and 1970s. These posttensioned trunnion anchor rods were used extensively for support of tainter gates and are considered the standard for the USACE and other government and nongovernment agencies within the United States and elsewhere. The older installed rods are now experiencing ongoing failures. The USACE needs reliable nondestructive testing (NDT) methods that are rapid, robust, and capable of detecting and quantifying defects, as well as methods for determining rod tensions. These methods are required to be rapid because of the large number of rods that exist at some installations. Robustness is required to handle the significant variations in design, construction, and field conditions that are known to exist. Defect detection and quantification provides tracking and monitoring data important for planning and prioritizing remediation efforts or operational practices.

1.2 Purpose of work unit

Research statements of need (SON) were submitted by the USACE Research Area Review Group (RARG) to the Navigation Systems Research Program. In response to these SON, a work unit (WU) was established to develop procedures and specifications to assess posttensioned anchorage capacity deterioration by means of microcrack detection using nondestructive testing/nondestructive evaluation (NDT/NDE) types of field techniques. The purpose of this research is to develop a field inspection capability for the purpose of detecting and quantifying slowly propagating cross-section loss due to microcracks in trunnion anchor rods. This inspection method would integrate into a scheme as shown in Figure 2.

Posttension rod loss is currently appearing as a rapid, brittle failure when a slowly propagating cross-axial microcrack reaches a critical level of cross-sectional area loss and crack intensity. For ungrouted rods, this has resulted in rods being ejected under extreme velocities. Heavy anchor plate housings have been constructed to help contain failing rods. It is not known if the defect growth and resulting rod failure rate will stay at its relatively low number of a relatively few per year across the USACE inventory or whether it will increase as older rods continue to be in-service and defects continue to slowly propagate until reaching a threshold total failure point.

Figure 2. Utilization of anchor rod NDT.

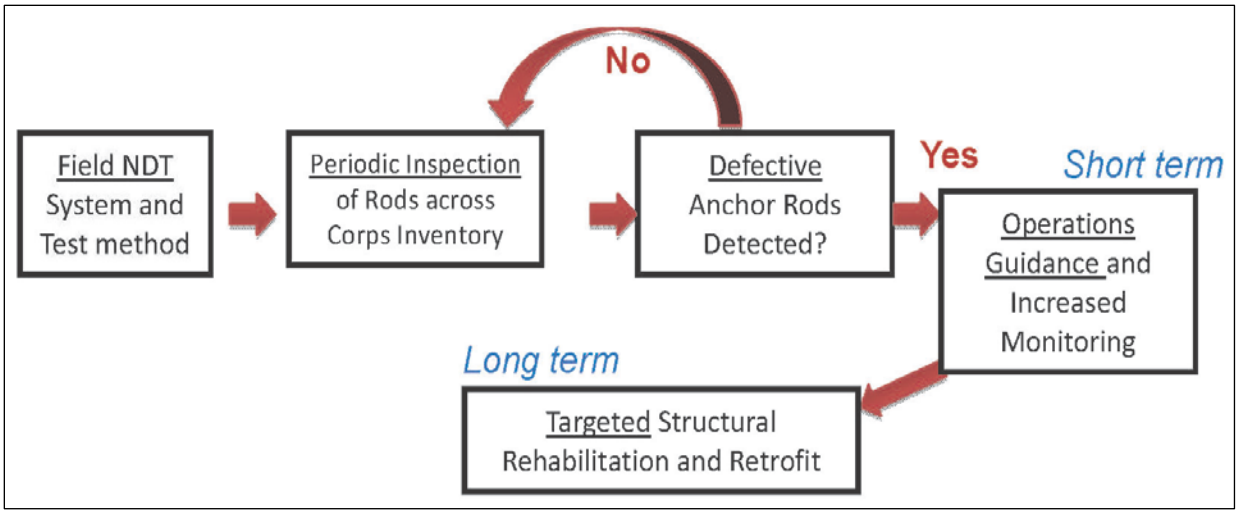

A successful NDT method will allow for rapid ultrasonic assessment and tracking of rod defects prior to their catastrophic failure. This effort leverages another ongoing project focusing on seven-strand steel cable failures whose origin is also from aging, early-design posttensioned steel systems.

The product of the trunnion anchor rod work unit will be to develop a test method and system specifications for successful realization of a system to provide detection of microcracks under the conventional field boundary conditions. These observed variations are important and, ultimately, will determine the specific mechanical response and testing accessibility/ conditions. The logistics-relevant system is described in the next section.

Research indicates that cracks, such as in fatigued rods, can go through opening and closing variations during their deterioration. Microcracked rods need to be detected and quantified regardless of whether the crack is in the open or closed condition. When a large crack is closed, the surface-to-surface *chatter* is higher, and hence, the nonlinear influence is greater. If a large diameter crack is pulled into the open condition, the nonlinear parameter becomes lower, but the linear detectability will increase. Because of this reciprocal influence with linear and nonlinear system detection capabilities, both are deemed necessary for robust microcrack detection. Hybridization is being pursued to facilitate robust detection and quantification of linear and nonlinear signal influences at significant downrange distances of opened and closed microcracks. Nonlinear-based detection must address and incorporate the influence of waveguide-based

dispersion effects, which define practical or desirable propagation modes. Tuned longitudinal and/or torsional propagation modes are currently being investigated in a full-scale test bed recently constructed at the U.S. Army Engineer Research and Development Center (ERDC). ERDC is also receiving technical support from leading researchers in the fields of nonlinear acoustics and guided-wave methods. The collaborators in these areas are Dr. Alexander Sutin of the Steven Institute and Dr. Joseph Rose of Feature Based Systems Incorporated.

A more detailed discussion of guided waves is included in the technical section later in this document, as well as information on the integration of guided-wave and nonlinear testing, which is seen as one of the technical challenges of this effort. The next section covers rod installation, design and construction variations, and typical embodiment.

1.3 Field conditions

EM 1110-2-2702 (HQ USACE 2000) is the current design standard and describes the use of posttensioned trunnion anchorage. The majority of the USACE projects used a trunnion anchor rod design, which requires the rods to be anchored to a metal plate embedded deep within the concrete spillway pier. Often, the rods are threaded into the anchor plate closest to the gate, with a protruding end that is commonly grouted into the mass concrete on the upstream side. The free ends extend through the downstream face of the pier, as seen in Figure 3b (below), and attach the trunnion girder to the pier. The exposed end is represented in Figure 3a with the protrusion varying from several inches to several feet. Often a removable cover box is used to protect this end from the elements. The number of rods required for a project is based on the size of the tainter gate and loading conditions. Across various designs and constructions, the tensile- and free-rod lengths also vary. Tensile-rod length sections are known to be as long as 70 feet (ft). The exposed ends also vary greatly from several inches to several feet with rough (welding torch cut) ends also being a common end condition. There is some but not much variation in rod diameter, with the majority of rod inventory being 1.25 inches (in.) in diameter. The tensioned section of the rod is typically encased in a 2 in. schedule-40 steel pipe, which is filled via injection ports with either thick anticorrosive grease (such as the current NO-OX-ID A special) or a cement-based grout. While newer installations use a threaded nut to load the rod, an older method, and more commonly seen, is a grip-nut assembly which uses a two-part compression wedge with serrated teeth to bite into the steel surface of a smooth rod. These

configurations are suspect to slippage and, as a result, are no longer used. The following section briefly describes lift-off testing, which is used as a calibration method or direct assessment of tension.

Figure 3. Typical exposed end of trunnion anchor rod (side view) in 3a. Figure 3b displays a schematic of trunnion rod anchorage from EM 1110-2-2702 (Figure 5-1) (HQUSACE 2000).

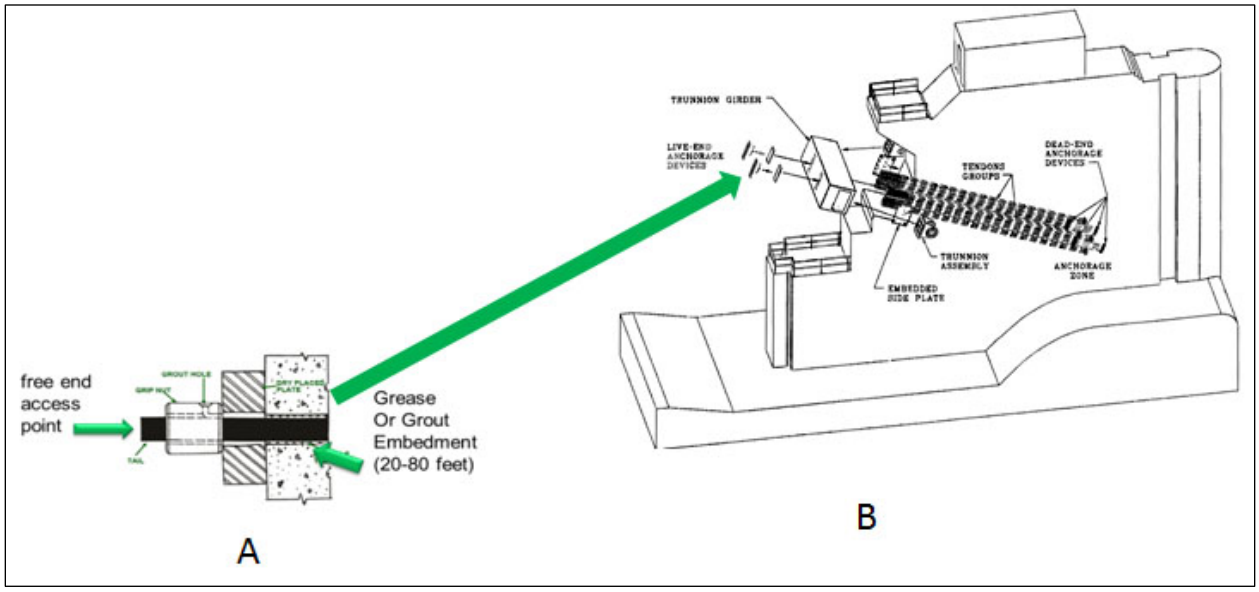

1.4 Existing technologies for defect detection

After high-strength posttensioned rods are manufactured, quality assurance testing is typically performed using one or more of various NDT methods. Typically, these are ultrasonic in nature, and examples include nonlinear modulation and time-of-flight diffraction methods, which are both used to detect very small cracks that might otherwise go undetected, even with conventional high-frequency ultrasound. Because of the obvious need to test trunnion anchor rods in-situ, rod accessibility becomes limited to only the exposed free end, and remote detection of very small defects becomes significantly more challenging. Commercially, no testing methodology exists that is capable of detecting open or closed microcracks in grease or grout-immersed steel rods at distances up to 60–70 ft away. The properties of the grease or grout surrounding the rod demand further consideration for system specialization and will be described in more detail later. At present, a commercial system is offered from Acoustical Control Systems (ACS) called the A1220 Anker, but its capabilities are limited to macroscopic cracks and defects at a range of 10 ft or less.

Passive acoustical monitoring technologies, such as acoustic emissions (AE), which listen for crack propagation noise within the material, are not seen as viable for several key reasons. They require expensive hardware that must run continuously and must be immune to background structural and electrical noise. There is no guarantee that the AE frequencies from propagation will not couple out of the rod and be below the threshold detection level. These systems seem better suited to high-count, posttensioned cables, such as the ones used on cable-stay bridges, where there is little attenuation (i.e., the cables are in air) and the system is attempting to detect total failure of a single wire and not propagation of a defect within posttension elements.

2 NDT System Development

2.1 Test bed

The posttensioned, trunnion-anchor-rod test bed was designed to allow for controlled laboratory testing under full-scale field representative conditions (Figure 4). The test bed allows for the tensioning of four rods across a length of 56 ft. Sleeve material consists of 2 in. schedule-40 pipe, as used commonly in the field, or oversized PVC, to avoid sleeve contact and allow larger immersion layers. Features include injection and access ports and internal embedded acoustical sensors.

Figure 4. Full-scale 4-rod test bed during construction and concrete placement.

Data presented in Figure 5 show an ultrasonic pulse echo on a 60 ft grease-injected rod using a piezoceramic transducer. Also captured in test-bed experiments were clear echoes from BB gun and hammer impacts. Obvious torsional wave echoes were also received from magnetorestrictive and piezoceramic transducers on the greased trunnion rod. These echoes present a beginning point for signal optimization, which can involve specification of frequency, propagation mode, transmitter, receiver, and postprocessing. More detail is presented below regarding propagation in acoustical waveguides.

2.2 Guided-wave methods

Unlike conventional ultrasonic inspection, guided waves allow for high-resolution defect detection and characterization at great distances from the applied transducer(s). These methods are well developed for a number of commercial needs including underground and/or coated pipes and rods.

Figure 5. Acoustical pulse echo from the end of the trunnion anchor rod.

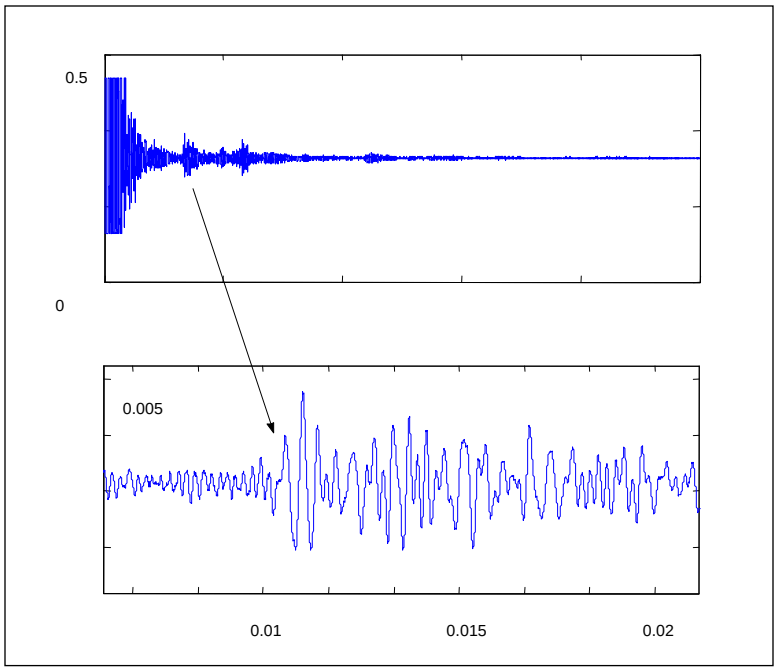

When inspection frequencies are high enough (e.g., when the ultrasonic wavelength is one-tenth the cross-sectional thickness or diameter), the propagation velocities can be treated like an ultrasonic wave propagating in a bulk material with no boundary influence (Rose 1999). At these frequencies, however, ultrasonic propagation characteristics such as attenuation, scatter, and inspection volume are typically poorly suited to detection of flaws at long distances. In general, waveguide structures such as plates, rods, pipes, and even more arbitrarily shaped extrusions like railroad tracks greatly affect the propagation characteristics of practical or usable ultrasonic frequencies. The cross sections, material properties, and surrounding materials together affect how the various propagation modes will perform at different frequencies. The cause of this frequency-based variation in behavior is due to the reflection, refraction, and mode conversions that are perpetually occurring at the material interfaces (Rose 1999). Graphs, called dispersion curves, are used to describe the various phase and group velocity changes that occur with respect to a changing frequency or frequency-diameter product. Note that the dispersion being described here is a wave-guide effect and not an intrinsic material property, as seen in some nonlinear materials. Phase velocity refers to the velocity of a phase point and is used in the development of tuned transducers and in the derivation of the group velocity curves. Group velocity refers to the actual movement speed of a wave packet down the length of the waveguide and is

used in determining distances to downrange reflectors such as defects or ends. Group velocity is actual reflected pulse velocity for a given frequency and mode of propagation. These modes and frequencies have in-plane and out-of-plane displacement characteristics that affect attenuation and cross-sectional sensitivity and are often exploited to either minimize propagation losses or control sensitivity at various cross-sectional positions. For example, for a pipe structure, a mode may be selected that minimizes the effect of fluid loading from a material that may be present within the pipe. Likewise, for an attenuative-surrounding material like grease or concrete, a mode may be selected which minimizes out-of-plane surface displacement and, hence, reduces signal loss. Energy velocity is basically group velocity curves where attenuation calculations have been included (Beard 2003). In determining an inspection mode and frequency, it is also beneficial to select a point of maximum energy velocity to limit the effects of dispersion and to reduce the risk of other modes complicating the detection of the received signal. Propagation modes can be either symmetric or antisymmetric in nature for compressional and shear wave propagation. The compressional or longitudinal energy is characterized by particle displacements that are parallel to the direction of propagation. In bulk material inspection, the compressional wave will travel almost twice as fast as the shear wave energy. The shear wave or transverse wave is characterized by particle motion that is perpendicular to the direction of wave propagation. In general, shear waves only exist in solids and are not carried in fluids. Some greases do have limited capacity in carrying shear waves. Because the viscosity of some greases will vary greatly with seasonal temperature changes, this is a parameter space that was explored under controlled laboratory conditions. In a rod-like structure, the shear wave particle displacements can either be in the radial direction (transverse shear) or parallel to the surface (horizontal shear or torsional). These two shear modes represent two very different guided-wave propagation modes. In general, with guided-wave inspection, the horizontal shear or torsional mode is usually the more desirable. This is because it is composed primarily of in-plane displacement, where there is very little mode conversion, and therefore, this propagation mode tends to be nondispersive and less attenuated by surrounding media. It has been described in the literature as being capable of *slithering* under clamps and other attenuative type bulkheads. The ability to place a torsional wave transducer all the way around the perimeter of the test piece helps to minimize the downrange sensitivity variations that can occur in torsional wave inspection. For pipe structures, focusing methods have been described, such as the total focusing

method and flexural torsional focusing (Sun et al. 2005), which can help equalize and, therefore, improve downrange flaw detection. Both the torsional and longitudinal wave modes were considered for inspection. Since the torsional wave travels near the surface, it is attenuated by contact with other media. In the subject case, this presents a problem since the rods are enclosed by either grease or grout. Shown in Figure 6 are torsional and longitudinal reflections from a shallow, 9 millimeter (mm) saw cut. This defect depth was 9 mm and was also detectable at 50 ft from the transducer-applied end. Plates, pipes, and rods are examples of simple guided-wave geometries.

Figure 6. Torsional and longitudinal reflections from a shallow, 9 mm saw cut.

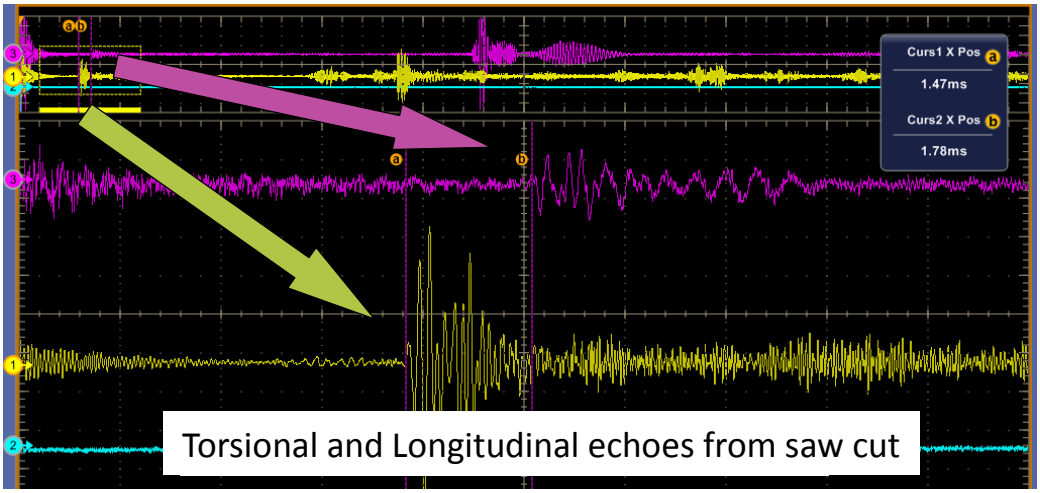

2.2.1 Rod waves

Studies by other researchers for defect detection in rod waveguides, such as rock and soil anchors, are well described in a number of papers (Beard and Lowe 2003; He 2006 et al.; Yang 2011). Commercial magnetorestrictive equipment is also used by the power industry in corrosional loss detection using guided waves for rods. Rod inspection favors longitudinal and torsional modes of propagation. The fundamental torsional mode for rod propagation does not undergo frequency-based waveguide dispersion, which makes it a good candidate for rod inspection. Additionally, the horizontal modes are well suited to slithering through bulkheads, sleeve contacts, etc. Generally, modes and frequencies can be determined for the specific inspection purpose desired. This is described for debonding of concrete, cladding, and insulation detection in papers whereby the more attenuated surface sensing frequencies have shown success up to tens of feet. The low-loss longitudinal modes, with lower surface activity, can

likewise be used for backwall detection and nonlinear measurements. The grease or grout is effective at coupling ultrasonic energy out of the trunnion rod and possibly into and back out of the 2 in. schedule-40 sleeve. Tools such as the Disperse guided-wave simulation software might prove valuable to identify rod echo frequencies that are not dominant in the 2 in. schedule-40 pipe sleeve. Examples of frequency sensitivity can be seen in the data in the following Figure 7, where a large clamp was placed just before a saw cut in a trunnion anchor rod. Analysis shows that the clamp reflected more energy near 25 kHz and the crack near 57 kHz. By tuning the system to 57 kHz, the crack could be detected without a false alarm from the clamp.

Figure 7. Narrowband tuning removes echoes from clamp, which simulates steel-on-steel contact.

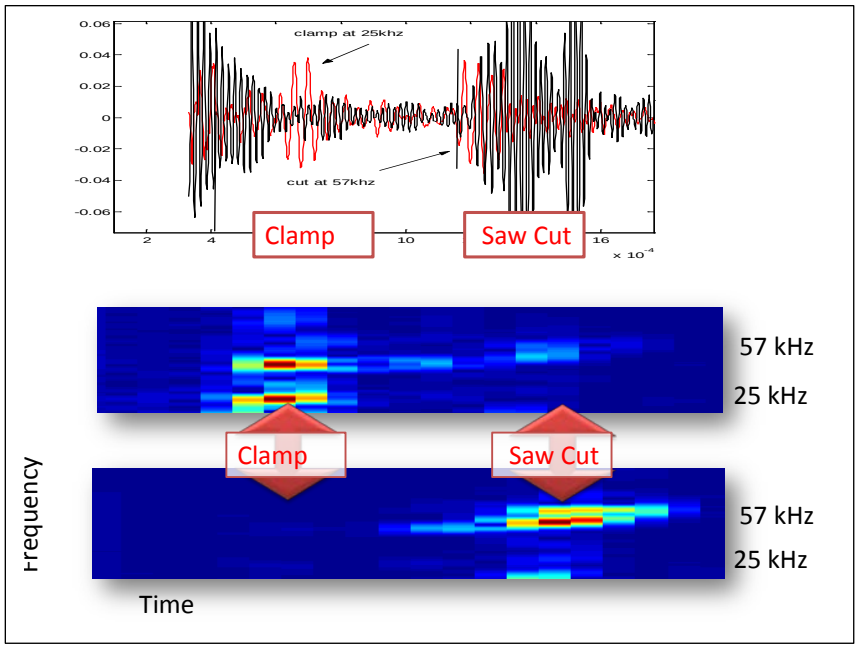

2.2.2 Higher-order longitudinal modes

The field boundary constraints of remotely detecting defects in an embedded rod with access limited to one end points to guided-wave acoustics as an NDT method. If these cracks are *closed* and hence poor reflectors, then nonlinear methods must be incorporated under the constraints imposed by guided-wave propagation in the element (Pruell et al. 2009; Jhang 2000). A number of investigators have covered rod-guided waves with the intent of solving problems such as rebar corrosion in concrete, rock anchor bolt bonding, and utility pole, guide wire anchor corrosion in soils (Beard et al.2003; Yang 2011; He et al. 2006). In general, these specific applications need high sensitivity at the rod surface and

therefore benefit from narrow-band, guided-wave modes such as low-order longitudinal or torsional modes that result in relatively higher levels of acoustical energy at or near the rod's surface. The drawback of these lower frequency modes is that energy leaks into the surrounding medium at higher rate producing correspondingly higher attenuation rates and therefore reducing the maximum testable rod length. Low-order attenuation cannot be overcome by simply continuing to apply more power because piezoceramic materials are limited by their dielectric breakdowns, or depoling, at extremely high voltages levels.

The trunnion anchor rod has an additional energy leak concern as the rods are typically 0.125 in. or closer to the steel sleeve that contains the rod and its corrosion-protection media of grease or grout. Test-bed experiments confirm that frequencies between 12 and 24 kHz tend to travel through the grease and propagate back and forth on the schedule-40 pipe. Propagation down these sleeves and their couplers or reflections from random rod/sleeve contact points would be a potential false alarm source if low-order longitudinal modes were pursued for inspection of embedded trunnion anchor rods.

Testing long lengths of embedded rods with vertical or horizontal shear modes is likewise problematic as these modes produce higher leakage into the surrounding medium and additionally suffer from higher material attenuation rates. Beard et al. (2003) and (He et al. (2006)) provide an excellent history of guided-wave mode development for rods and proceed to demonstrate that for long distances inspection, higher-order longitudinal modes are the best solution. This is because energy becomes more and more centralized in the rod, and leakage rates at the surface are reduced proportionally. As frequency continues to increase, material attenuation rates also increase, and so a point of diminishing return in encountered. Figure 8 illustrates the principles behind the high-order, low-loss propagation modes. The increased energy centralization that occurs at higher frequencies (i.e., higher longitudinal modes) minimizes surface displacements and energy leakage into the surrounding medium. The limitation of what can be gained from energy centralization occurs at higher frequencies where the material attenuation begins to impede ultrasonic propagation. An example portion of low loss range of longitudinal modes in a 1.125 in. bar is shown below the two superimposed gain curves.

Figure 8. Low-loss modes existing between centralization of guided-wave energy at higher frequency and lower material attenuation at lower frequencies.

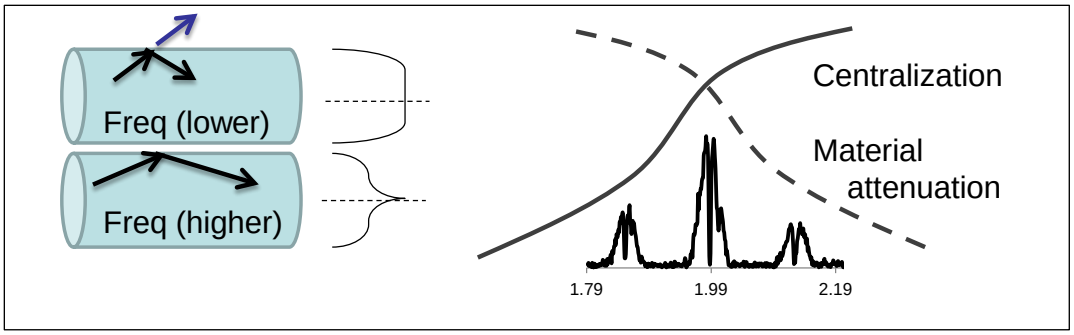

Figure 9 illustrates an experimentally collected, broad-band energy velocity curve for various embedded rod modes in Figure 9 (left) and the higher frequency and sustained modes in Figure 9 (right) that were captured in multiple reverberations. These higher-frequency modes in the 1 to 3 MHz range are the most practical for long-distance trunnion anchor rod testing. The time frequency plot's A-scan is shown above the spectrogram in Figure 9 (right).

Figure 9. Energy velocity curves showing compression and torsional modes (left). Reverberation of high–frequency, low-loss modes and the associated A-scan (right).

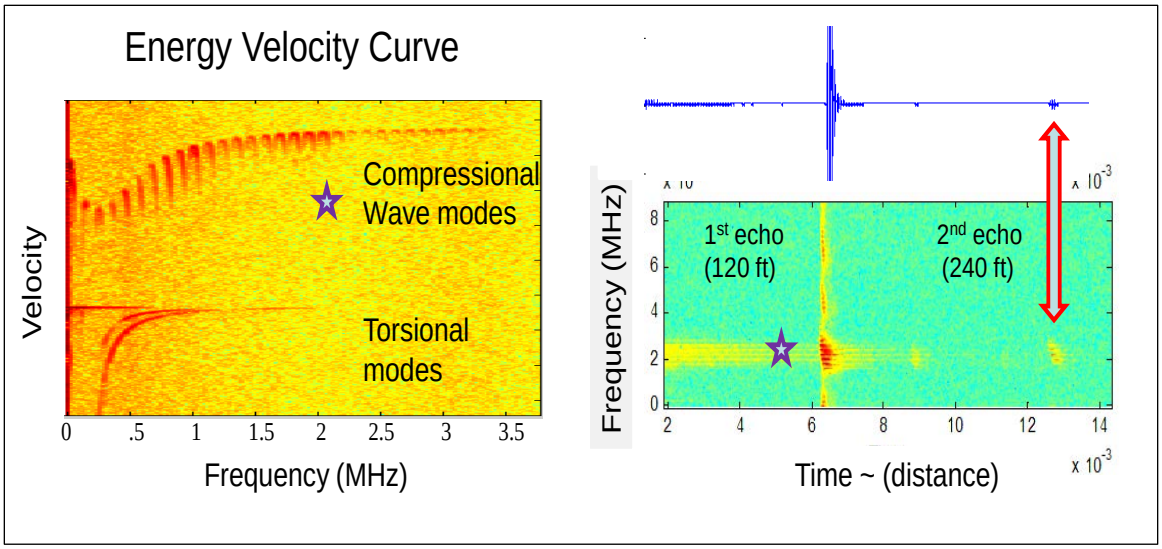

To evaluate the capabilities of shallow, near-surface defect detection, an experiment was performed where a progressively deepening cut was made while monitoring the expected reflection region in the ultrasonic A-scan. This cut notch was detected with an approximate signal to noise ratio of 2 using the low-loss, narrow-band inspection frequency at a depth of 0.1 in. at a distance 23 ft away from the free end of a grease-embedded 1.2 in.

diameter rod (Figure 10). As the cut was increased, the echo amplitude grew as expected at a very high rate due to both the increased rate of material removed from the rod's cross-section and the reflection of the higher energy concentrations as the cut moves towards the rod's center. The spectral signature of the cut (i.e., open crack) can serve as a signature for monitoring purposes.

Figure 10. Narrow-band spectral reflections at a 0.18 in. deep cut and the rod end of a 1.31 in. diameter grease-embedded trunnion anchor rod with concrete termination.

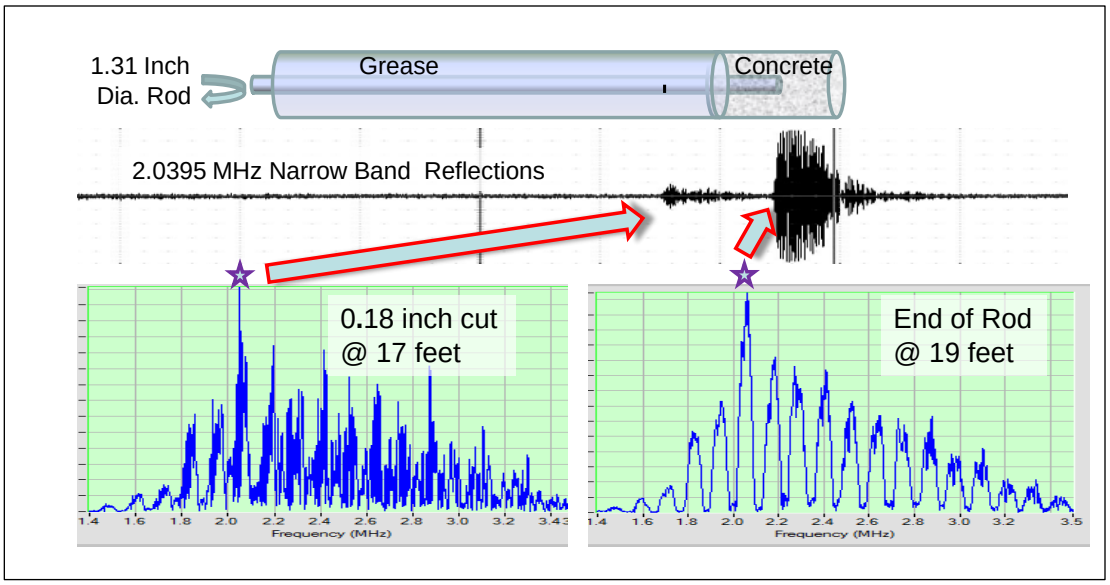

2.2.3 Physical propagation influences

Rod diameter has a significant influence on the ultrasonic attenuation rates as well as the frequency spacing and location of the low-loss modes. Comparison of rod diameters that are 1.25 in. and 1.125 in. results in an attenuation rate increases by a factor of 3 for the smaller diameter rod. According to EM 1110-2-2702 (HQUSACE 2000), a 1.0 in. rod is the minimal allowable rod diameter for tainter gate anchorages. Seven-strand cables are also used at some dams. At present, cable inspection lengths are limited to 12.5 ft at a low-loss mode of approximately 5 MHz In its current state, the ERDC guided-wave system can inspect the more attenuative 1.125 in. grease-embedded anchor rods at lengths of over 100 ft. Because of the low surface leakage, the grout embedding medium results in only a minimal increase in attenuation when compared to grease embedment. This has been verified in test-bed experiments, and additional technical detail on embedding medium influence on higher frequency modes is given by Beard and Lowe (2003). A high-power/high-sensitivity piezoelectric material,

manganese-doped lead indium niobate-lead magnesium niobate-lead titanate (Mn PIN-PMN-PT) (Luo 2009), was evaluated but was found to be band-width limited. This new piezoelectric material is reported to potentially produce gains up to a factor of 8 over commercially available, high-performance lead zirconate titanate (PZT) materials.

Experimentation has demonstrated that both *rod tension* and corresponding bulkhead loading have a negligible influence on the propagation of low-loss modes. Other physical rod characteristics, however, should also be considered as their influence can be quite significant. Rod *end condition* is a significant influence and can vary in terms of both angle and smoothness.

2.2.4 Nonlinear investigations

In order to improve detection capabilities beyond the current limits, efforts were made to utilize nonlinear acoustical methods. Initially, these experiments were carried out on various small rods across a variety of frequencies. In later efforts, an initial attempt was made to integrate a nonlinear inspection method with the guided-wave inspection frequencies previously described. As there is a wide variety of potential nonlinear methods, other hybridization strategies remain unexplored. Two major difficulties experienced in this phase of the investigation were 1) minimizing nonlinear influences from the transducers and 2) developing representative engineered defects for investigation. Details of the nonlinear investigations are included in Appendix A.

2.3 Greenup Lock and Dam field testing

Initial investigations in this research effort established proof of concept for remote, closed-crack detection using nonlinear methods. In the second stage of this research effort, linear guided-wave methods have been developed and evaluated to obtain end-of-rod reflections for the high rate of attenuation present in full-length grease- and grout-surrounded rods.

Rick Haskins and Ken Switzer performed tests at Greenup Lock and Dam during the week of 26 March 2013. These tests were performed in support of the Navigation Program Trunnion Rod Research Program at ERDC. The Greenup Lock and Dam inspection served to evaluate the field performance of acoustical guided-wave test methods on in situ rods. Additional background information relating to these rods and the initial ERDC

research efforts aimed at development of a nondestructive method of inspection is provided in ERDC/CHL CHETN-IX-32 (Evans et al. 2013).

Test-bed-based investigations have also addressed influences from tension, end conditions, and methods for frequency and mode determination. Laboratory experimentation confirmed that the current system is capable of detecting a 0.1 in. deep open crack in a 1.3 in. diameter embedded rod at a distance exceeding 50 ft. The next stage of this research will integrate these techniques to produce a system capable of detecting microcracks in trunnion anchor rods throughout their evolution. The higher-order, ultrasonic, guided-wave inspection testing approach being developed at the ERDC test bed proved successful for inspection of the highly attenuating trunnion anchor rods at Greenup Lock and Dam. Initial on-site frequency scans were used to determine the specific low-attenuation, narrowband, guided-wave propagation modes best suited for pulse-reflection measurements and their variability.

At Greenup Lock and Dam, the small diameter (1.125 in.) and longer length (80 ft) rods make the end-of-rod echo detection case there a worst-case scenario. Findings from the Greenup Lock and Dam testing, along with laboratory measurements, have been used to design an improved system which will enhance the effective dynamic range of the digitizing hardware, enable further reduction of nonstationary noise, and optimize echo detection along the entire length of the rod. The dynamic range improvement from this modified system will aid in the implementation of guided-wave-based, nonlinear methods such as gated frequency mixing, harmonic analysis, and impact modulation for closed-crack detection.

2.3.1 Tension testing

A 2012 follow-up flexural vibration-based test, which used pull-off mechanical load testing and empirical computer modeling to develop correlations between measured-rod, low-frequency (LF) flexural vibrations and a rod-tension state, was also recently performed at Greenup Lock and Dam by a private NDT company (Cesare et al. 2012). Results of the second investigation have just been published at the time of this writing. The first tension analysis relied on a number of assumptions due to the lack of pull-off data for correlation. The second analysis compared empirical modeling and load-test results to explore the possibility of three-dimensional (3D) finite element modeling (FEM) as a means to avoid

pull-off requirements. It is important to note that this LF, vibration-based approach is not expected to be sensitive to the presence of a closed or open microcrack for the following reasons: 1) an open crack will not produce a detectable change in rod tension given the modulus of steel and realistic size crack openings and 2) while a crack would affect the low-load-dominant, cantilever-vibration mode where the restoring force is a function of the material properties and geometry, a crack will not significantly change the taught-string vibration mode which is dominant at trunnion-anchor operational loads. Preliminary results from this effort indicate that cantilever length, material modulus, and grip nut contact can have significant influence on the dominant measured frequencies when compared to the influence due to tension.

2.3.2 Guided-wave tension influence

Using modulus relations with estimated entities of diameter and length, it is estimated approximately 0.3 in. of rod stretch per 10,000 pound (lb) variation in load. This would indicate that at a sample rate of 100 MHz, a shift in pulse arrival time of approximately 250 samples (or 2.4 microseconds) would result as the roughly 19,000 feet per second (ft/sec) pulse traveled through the stretched length twice (incident and reflected). This indicates a potential high level of differentiation in detected changes in rod length caused by changes in tension.

Also considered were diameter changes relating to tension which would be promising as the diameter influence on guided waves is clearly observed in the frequency spacing of low attenuation modes. Poison's ratio indicates that the diameter will only change by approximately .0013 in. over the rod's elastic range, which is too small to discern in mode spacing in the frequency domain. The observed echo shifting due to length changes at Greenup Lock and Dam was larger by at least a factor of 2 than what could be explained due to nominal tension variations. It is likely that there is additive influence from variations in delivered rod lengths. The ERDC guided-wave method appears to be extremely sensitive to *changes* in tension due to the short wavelength and high sample rate being used. A method of intersecting guided-wave modes was developed in the test bed that provides a robust, simple, and repeatable method of time-of-arrival estimation on a given rod. This method is also well suited to real-time monitoring methods using active acoustics. An example is given at the end of the following section as well as results from tension-based, guided-wave investigations performed in the ERDC test bed.

2.3.3 Pre-Greenup Lock and Dam ERDC test-bed investigations

A failed small diameter rod of approximately the same diameter (1.25 in.) as the Greenup Lock and Dam rods was recovered from a vertical miter-gate, posttensioning pier. This rod proved valuable in pre- and post-Greenup Lock and Dam investigations as well as general investigation on the influence of diameter variations. This section of the report covers group velocity, attenuation, and tension investigations performed at the ERDC test bed in preparation for Greenup Lock and Dam field testing.

Using a grease-encased laboratory rod of similar diameter at the ERDC test bed, the group velocity at the lowest-loss inspection frequency was estimated. The Greenup Lock and Dam rods were on average 1.1425 in. in diameter, and the ERDC posttension rod was slightly larger at 1.16 in. It should be noted that the cold-rolled, posttension rods, whether large or small, are not perfectly round, and the diameter appears to vary by 1% to 3%. The laboratory rod was used to develop an understanding of the group velocity at the target inspection frequency.

Guided-wave inspection using narrowband pulse energy consists of two velocity properties for a given frequency and mode of propagation. These are the phase velocity, which is the speed of the high-frequency (HF) transmitted energy traveling along the test object, and the slower group velocity, which is the slowly changing envelope of the transmitted pulse. The group velocity can be thought of as the actual information signal, and the entity which, during pulse-echo measurements, is used to describe the time of arrival and, therefore, to determine the distance to various reflectors. In bulk material testing, these two entities are the same; however, in acoustical waveguides, they generally are not the same (the exception is the fundamental torsional wave mode). The group velocity is slower than the bulk material velocity because it is developed from multiple reflections and refractions from the waveguide surface. In movement from lower to higher frequencies of low-loss propagating modes, the group velocity of mode peaks generally increases. For the optimum low-loss modes in the larger 1.25 in. and smaller 1.125 in. (design specs) test-bed rod (Table 1), the group velocity is approximately 18,691 ft/sec and 19,000 ft/sec, respectively. This estimated 19,000 ft/sec group velocity, based on laboratory measurements, was used to estimate a typical Greenup Lock and Dam rod length of approximately 81.7 ft. This measurement was in agreement with Greenup Lock and Dam blueprint drawings.

Table 1. Low attenuation modes for various rod diameters.

Average	Optimum
Rod Diameter (inch)	Frequency (MHz)
1.1425	1.986
1.159	1.957
1.3125	2.175

Attenuation studies on the small-diameter, test-bed rod were also performed prior to the Greenup Lock and Dam inspection. In general, the grease and grout surrounding in situ, posttension anchor rods will *drain* the ultrasonic inspection energy from the rod. For vertical and horizontal (or torsional) shear wave energy, this effect is worsened by their higher intrinsic material attenuation. For the higher-order (higher frequency) longitudinal modes in the L(0,9) to L(0,12) range, the ultrasonic energy becomes more centralized in the rod, and very narrow bands of frequencies can be found where there are minimal surface displacements. This lower surface displacement results in relatively much lower attenuation rates (Pavlakovic et al. 2001). Laboratory testing has validated that these low-surface energy modes are still capable of detecting very shallow defects at great distances downrange. These tuned modes also avoid the issue of coupling energy into and out of the steel pipe sleeve containing the rod which would otherwise generate false backwall echoes. Additionally, the bulkheads and sleeve contacts do not tend to significantly drain or reflect these higher-order modes either. As the frequency continues to increase, the intrinsic ultrasonic material attenuation also increases. This creates a point of diminishing return or an optimum inspection point between the improvement in energy centralization as frequency is increased and the reduction in material attenuation as frequency is reduced.

Using relative amplitudes of first, second, and third reflections, a grease-embedded attenuation rate was estimated for the various rod diameters. For the smaller Greenup Lock and Dam rods, an attenuation rate as high as 0.6 decibels per foot (db/ft) per propagated length was measured. This means the amplitude of the reflected signal is halved for every 2.5 ft of rod length (2.5 ft (rod length) × 2 (two-way dist) × 0.6 (db/ft) = 3 db). This estimate did not incorporate the small end losses which occur due to mode conversion when the signal reflects off the end of the rods. The larger diameter 1.31 in. rods exhibited significantly less attenuation at their low-loss mode, with attenuation rates being approximately 0.2 (db/ft). For a 0.125 in. reduction in rod diameter from the more common 1.25 inch

rods, the attenuation rate is tripled. These high attenuation rates challenges are being compensated for with customized amplification circuits discussed in a latter section of this report. The Greenup Lock and Dam rods exhibited approximately 96 db of attenuation for the approximate 160 ft of signal propagation.

Test-bed investigations were performed to evaluate the influence of tension on the inspection frequency and HF, guided-wave propagation modes. As the rod length increases due to tension and the modulus of elasticity, the wave also propagates a longer distance. This relation for the rod is described by its modulus (31.6×10^6) which is equal to stress over strain, where strain is the change in length over initial length and stress is the force per unit area. The specified area is 1.25 square inches (sq in.) for the tensioned rod; however, the rod is more typically 1.31 in. in diameter which gives it an area of 1.347 sq in. Aside from making the rod longer and proportionally delaying the backwall echo, no other significant influence was determined. The spectral scans showed no detectable frequency change across a broad range of applied tensions. There are both positive and negative aspects of this. On the positive side, the selected inspection frequency is robust and will not change significantly as load variations fluctuate. On the negative side, this spectral amplitude information is not likely to be a useful mechanism for indication of applied load. Figure 11a shows the pulse delay from varying load on the dominant inspection frequency as the load is increased to 140,000 lb. Figure 11b shows the intercept of three sequential, low-loss frequency modes across the same variations in load. Note that this intercept provides a consistent marker for tracking the changes in load in a real-time-monitoring scenario. Also note in Figure 11b that the lower-frequency modes arrive significantly more slowly (red pulses) and the higher frequencies (blue pulse) arrive sooner.

2.3.4 Guided-wave testing at Greenup Lock and Dam

Because of the height and narrowness of the ladders, it was deemed impractical to transport the laboratory electronics down to the location of the trunnion anchor rods. Figure 12 shows the relative locations of the transducers and electronics. A small preamplifier was used to offset the influence of the return signal path.

Figure 11. Variation in load and the resulting influence on propagation delay.

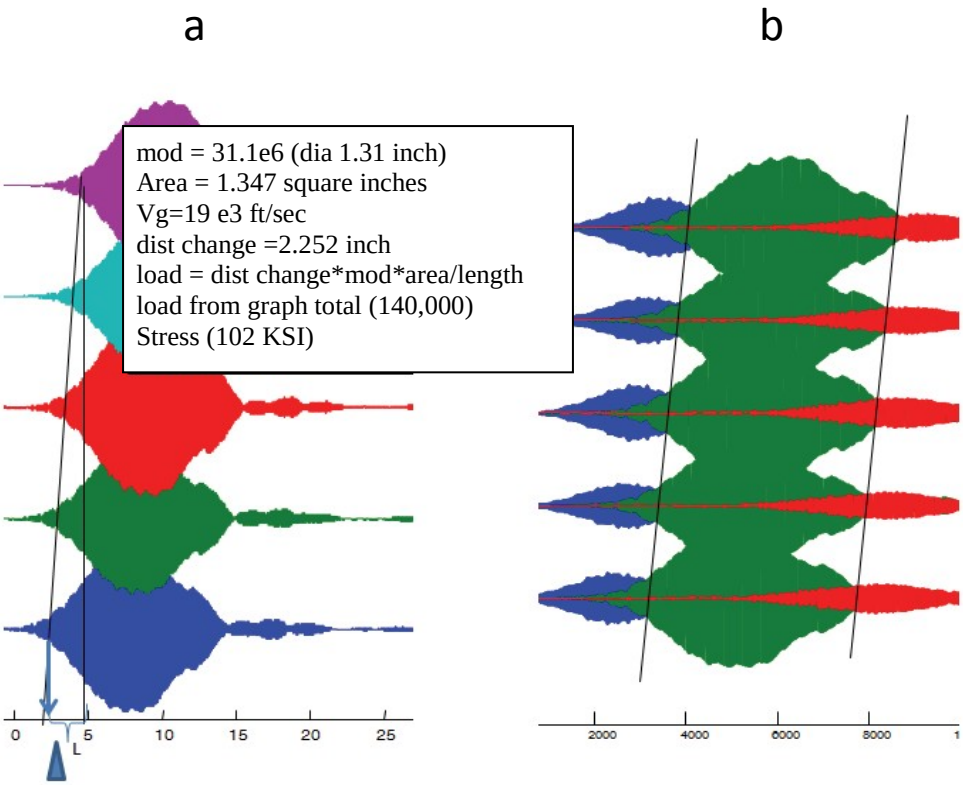

Figure 12. Location of testing equipment at Greenup Lock and Dam.

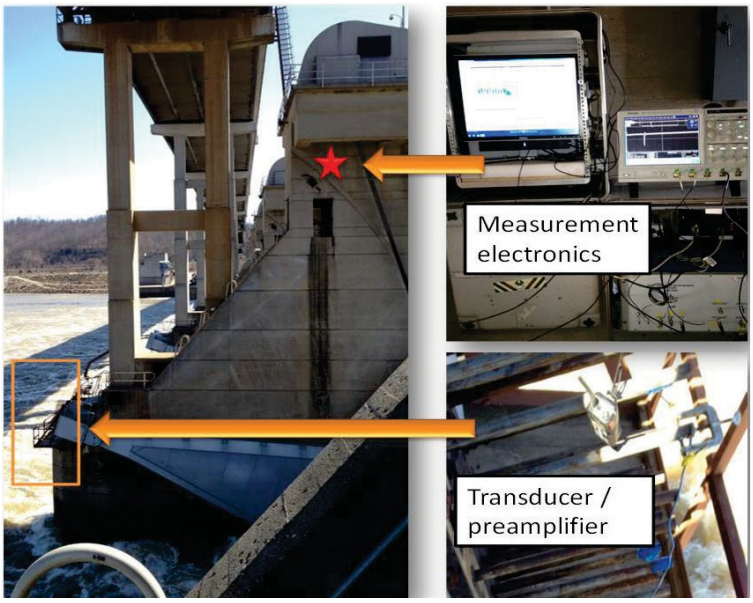

Prior to narrow-band testing, numerous frequency scans were performed on randomly selected rods in each bank to determine the ideal guided-wave inspection parameters and to verify their consistency from rod to rod. Three of these frequency scans are shown in Figure 13. For the majority of tested

rods, the backwall echo was obtained using 200 cycles of 1.9865 MHz ultrasonic energy. These parameters specify a lowest-loss, high-order longitudinal guided-wave mode for echo detection for the Greenup Lock and Dam rod and system configuration used. For a bank of rods which performed poorly to this frequency, additional testing was performed at a slightly higher center frequency (1.995 MHz).

Figure 13. Three frequency scans at Greenup Lock and Dam and the selected low-loss inspection mode.

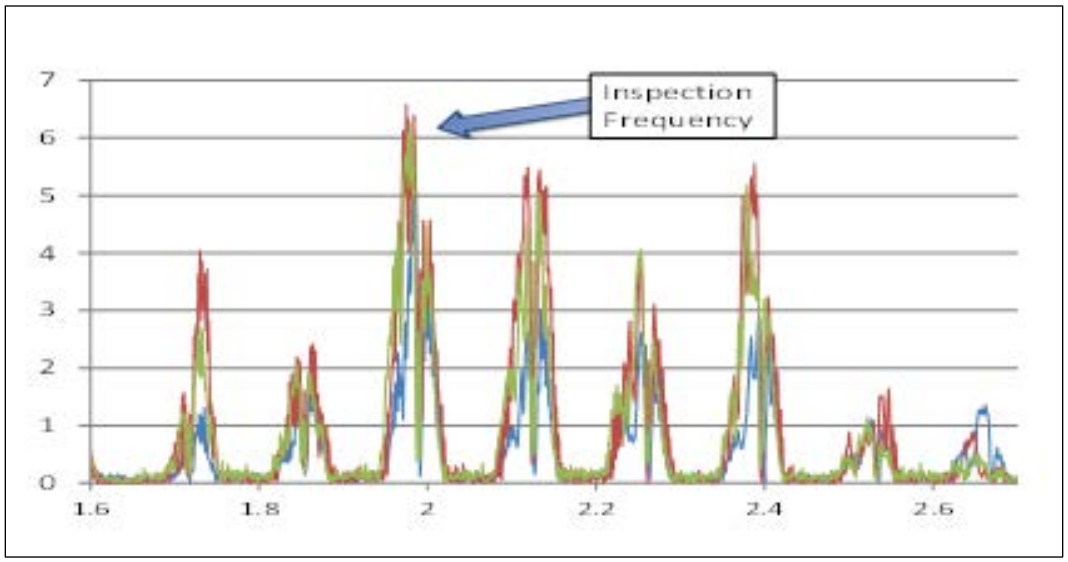

While the rod ends at Greenup Lock and Dam were factory cut and nearly flat, there was a consistent high-edge artifact present from the factory finishing process. This small edge prevented ideal flat placement of the 1 in. diameter transducer. This small edge was easily and quickly removed with a flapper-type rotational sander. The very long and highly attenuating (small diameter) rods at Greenup Lock and Dam demonstrated the need for dynamic range enhancement of the system. In other words, to properly digitize the weak and attenuated backwall reflection, a large amount of signal gain (78 db at Greenup Lock and Dam) had to be applied, which had the net effect of over-amplifying the ultrasonic backscattered energy in the front end of the signal. This saturation of the initial signal information is shown in Figure 13. To minimize the loss of echo information in the received signals, they were clipped well after the first backwall echo with the goal that any near transducer reflections from cracks could be picked up as the signal propagated back down the rod for the second time (i.e., to the right of the first end of rod reflection). The over saturation section is clipped in the remaining Greenup Lock and Dam data presentation. An improved solution to these problems is covered in the next section.

In addition to the RF signal shown in Figure 14 (left), a heterodyne phase-detected signal was also digitized from the RITEC's output. These data are effectively a narrowband signal filtered to the transmitted frequency and amplitude-demodulated with respect to phase. This circuit can be very useful for improving the signal-to-noise ratio and stripping away the HF carrier (or characterizing the envelope of the reflected energy). Figure 14 (right) shows the reflected backwall pulse in both RF and phase-detected forms. Note that the RITEC's analog phase detector will also be useful in future nonlinear acoustical experiments as it can detect and characterize (via integration) various harmonics and signal mixing (from its two independent pulsers).

Figure 14. Typical signals showing front-end information loss due to high gain required for echo detection (right is zoomed in with overlaid receiver's phase-detected signal shown in green and radio frequency (RF) pulse shown in blue).

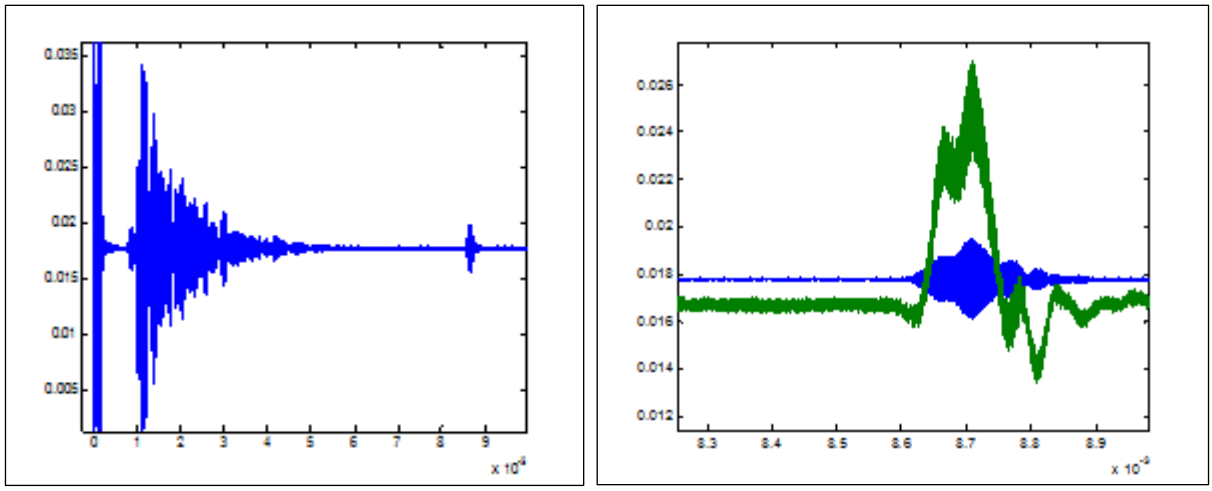

Figure 15 shows various representations of some of the signals collected at Greenup Lock and Dam. The center image in Figure 15 shows zoomed-in, phase-detected signals from the east-most pier. The circled region in the center panel shows rods that had weak backwall reflections and were rescanned and retested with a slightly higher inspection frequency. The figure on the right in Figure 15 shows the retested data zoomed in to the backwall.

Figure 15. Various representations of some of the Greenup Lock and Dam test data. The *x*-axis is time in milliseconds (msec).

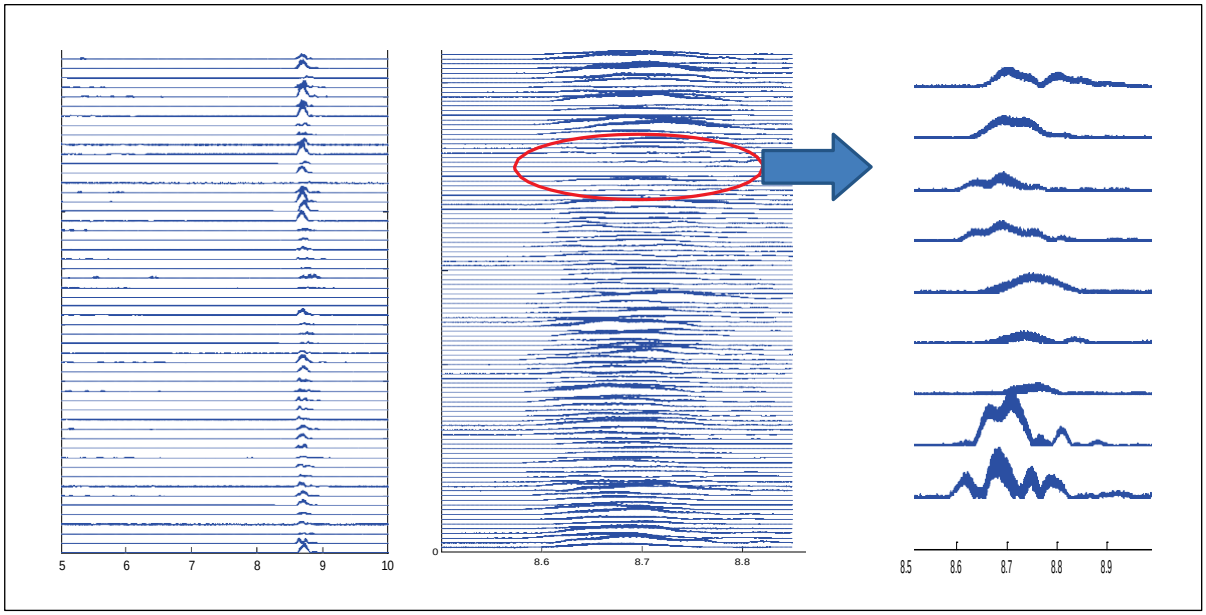

The shift in ideal inspection frequency seen in the lower section of the far-east bank of rods corresponded to a migration of the dominant peak from the left to the right of the null point in the low-loss frequency mode. This null point consistently appears in low-loss propagation modes and has been commented on by other guided-wave researchers (Beard 2003). Figure 16 shows this low-loss mode frequency migration in the spectral domain. The solid lines correspond to rods where the ideal inspection frequency shifted to the right of the null point. The new low-loss mode for this small subset of rods is approximately 1.995 MHz. This change observed in this small group of rods is suspected to be due to either material property variations or curvature in the rod axis due to sleeve contact. Research (Beard 2003) indicates that curvature as small as 800 times the rod diameter can be detected in guided-wave responses.

2.3.5 Post-Greenup Lock and Dam system optimization

Three primary system improvements were determined and implemented following Greenup Lock and Dam testing. These improvements included a preamplifier, a time-compensated gain circuit, and a more powerful transducer.

Figure 16. Shift in ideal inspection frequency as observed for a group of rods (pier 2, east bank).

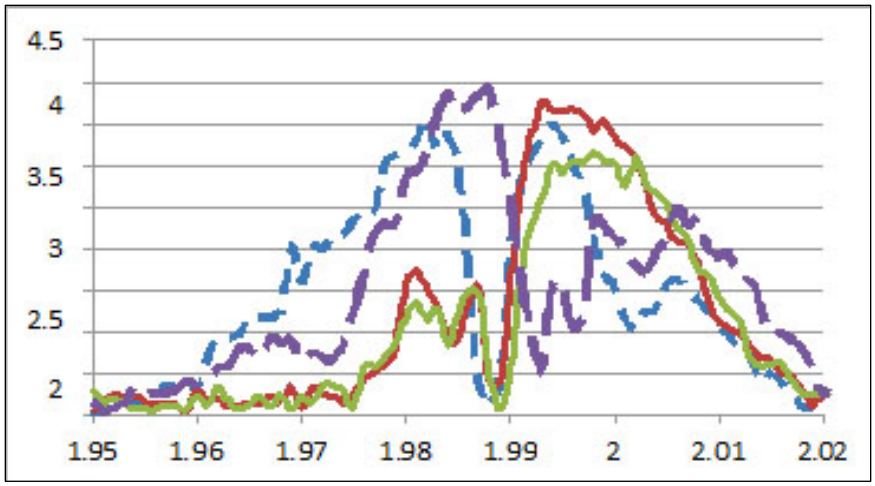

Part of the initial signal loss observed at Greenup Lock and Dam had to do with the slow saturation recovery of the Olympus, Inc., preamplifier after the initial high-power pulse was transmitted. A high-pass filter was used to minimize this effect prior to digitization. Some of this saturation effect can be seen in Figure 14 (a) in the flat section of the signal before the 1 microsecond (µsec) mark. A RITEC amplifier was used in test-bed evaluations and was seen to exhibit 100 times faster settling time and, therefore, allowed recovery of this initial section of the signal. The improved recovery corresponded to 33 µsec settling time instead of the 3000 µsec seen with the Olympus preamplifier. Because the RITEC amplifier has inferior noise characteristics and is not battery powered, a new ultra-low-noise preamplifier with even faster recovery than the RITEC amplifier is being incorporated into the latest system design.

New transducers arrived shortly after the Greenup Lock and Dam field test and were evaluated on the small-diameter laboratory rod. The transducer used at Greenup Lock and Dam was a low-hat, dual-element design which has very low damping. This low damping is advantageous because it results in more detection sensitivity as well as ultrasonic power output. However, the low damping and quarter-wave matching layer were observed during impulse stimulation to produce several undesirable in-transducer reverberations every 6 µsec as the pulse bounced between the steel test surface and peizoceramic transducer. During guided-wave, tone-burst measurements, these reverberations produce undesired interference effects. A new 1.5 in. diameter, medium-damped PZT, ceramic-based crystal (i.e., an Accuscan model by Olympus) was seen to produce even better results

without the interfering in-transducer reverberations. Because this transducer is more broadband than the dual-element design, it also allows a slightly wider window of candidate low-loss inspection modes. Figure 16 shows the improved signal levels from multiple reverberations of the 19 ft × 1.125 in. greased rod at ERDC. The circled echoes in Figure 17 correspond to the propagation length of the Greenup Lock and Dam rods. These signals have been amplified with the time corrected gain (TCG) circuit discussed next.

Figure 17. Improvement from Accuscan transducer over dual element used at Greenup Lock and Dam.

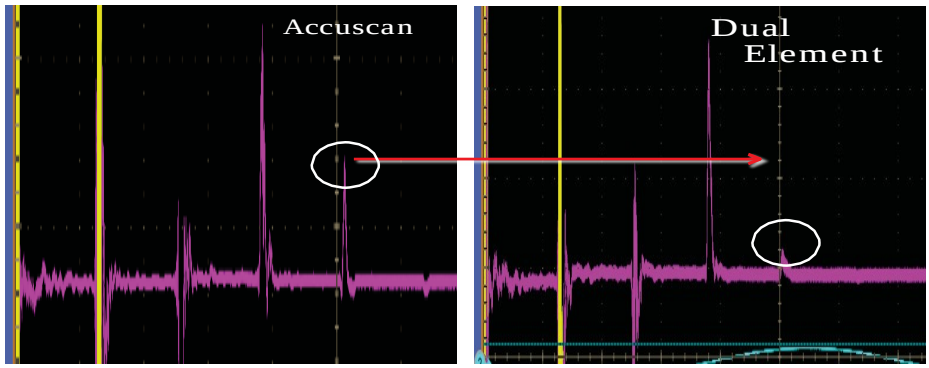

Ultimately, several solutions to the dynamic range problem are possible, including signal integration across either various gains or pulser-output levels. The most elegant and common approach (used in radar and other range-dependent attenuation systems) is to use a (TCG) circuit, which allows the operator to dial in a gain function that increases with time (propagation time). The ideal gain function was seen to be a sine wave which starts at negative 90 degrees phase and ends at positive 90 degrees phase at the last detectable end-of-rod or backwall echo. This circuit adds some complexity to the system as it must be triggered in synch with the pulser and provided with an appropriate gain function. Currently, a 12-bit waveform generator is being used to apply the signal gain function. To date, three TCG integrated circuits have been evaluated, and another is on order. The best performers have allowed for negative gain (i.e., attenuation) of the front portion of the signal and had a wide gain function (60 db). Tests on near-transducer rods cuts were also evaluated to make sure that detect-ability in this range was not hampered. The TCG performed well in these evaluations. Using measurements on the 19 ft Greenup Lock and Dam representative rod, Figure 18 shows the front-end saturation as seen during field testing (top signal) and the improved signal after applying the TCG amplification (bottom signal).

Figure18. Top signal shows Greenup Lock and Dam setting and front-end saturation for the representative small laboratory rod; the bottom signal shows the improvement after TCG application.

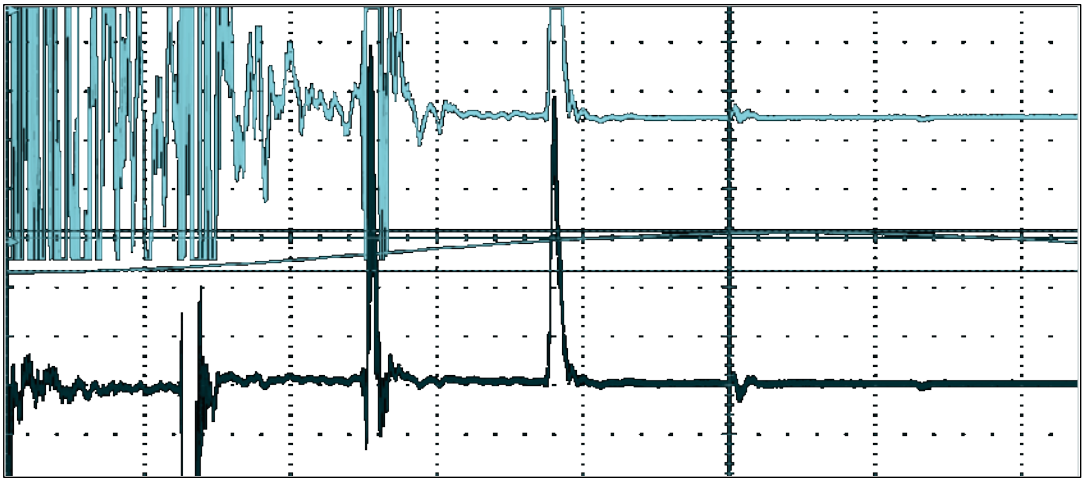

After inclusion of the TCG circuit, various system configurations were explored to determine the optimal configuration and settings of the various components. It was determined that the TCG circuit performed better with some degree of pre-amplification and that the TCG circuit produced the best results when applied before the RITEC's phase detector. The final optimized circuit is shown in Figure 19. As noted earlier, common triggering between the function or waveform generator, the TCG circuit, RITEC system, and oscilloscope is required. Efforts are underway to integrate the function generator, TCG, and preamplifier circuits into one unit with simplified controls for field setup.

Figure 19. Block diagram of optimized system configuration.

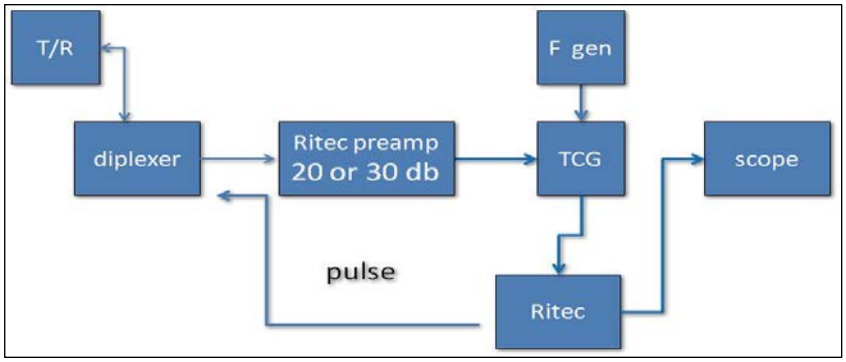

2.3.6 Results and conclusions from the Greenup Lock and Dam effort

The ERDC trunnion-rod microcrack detection system is still in its development stage, and this Greenup Lock and Dam inspection trip was primarily intended to evaluate the robustness and field performance of the

guided-wave methods being developed at the ERDC test bed. In general, good agreement was found between the data being collected on embedded laboratory rods at ERDC and the field data collected at Greenup Lock and Dam. Some differences in optimal setup were observed, such as the use of a diplexer pulsing one large element was seen to perform better at ERDC, while a pitch-catch configuration using two half-sized elements without a diplexer performed better in the field. This observation, however, may have been contributable to the preamplifier saturation problem discussed in the previous section.

The 200 rods at Greenup Lock and Dam were successfully tested, and a backwall signal was received for each one. These long-length and small-diameter rods presented a challenging high-attenuation case for trunnion anchor rod testing. No defect echoes were detected in the observable parts of the signals. A small group of rods on the lower section of the east bank of pier 2 produced weak end-of-rod echoes. Retesting at a slightly higher frequency improved the amplitude of echoes from these rods, but only marginally. It is not known what created the effect, but the following theory is put forth: the rods may be contacting the containing sleeves to the point of causing a small degree of rod deflection and, hence, destructive guided-wave phase interference.

Significant improvements have already been made to the system and configuration used at Greenup Lock and Dam. Tentative plans are to return and re-inspect these rods with this new system configuration. The new transducer and gain circuits are expected to provide significantly stronger end-of-rod reflections while also allowing acquisition of data from the front section of the rod. This information was previously lost due to amplification-related issues discussed in this report. Additionally, improvements have also been made in finishing the rod ends so that better transducer coupling is assured.

This report also addresses the influence of rod diameter on guided-wave attenuation, group velocity, and spectral mode spacings. Tension and length variations were also addressed, and a proposed methodology of robust time-of-arrival tracking was presented towards development of an in-place, active tension/defect monitoring system.

3 NDT System Operation and Components

3.1 Test method of current system

An optimized system hardware configuration detailing the relative location of these components was determined following the Greenup Lock and Dam testing. The current process used for the optimization of system operational parameters forms the beginning of a test method for open crack detection. In its current state, the overall method for testing at a new site is as follows:

1. Inspect rod end conditions and perform quick tap-test survey. If rods need end *dressing*, use a portable band saw and a belt sander along with a removable steel guide collar to achieve a smooth orthogonal end condition.
2. Perform frequency scanning of the end-of-rod echo gate from approximately 1 to 3 MHz with the transducer clamped to rod end to determine optimum low-loss propagation modes. This should be performed on several rods within each anchoring group to assure consistency.
3. After visually determining an optimum low-loss mode from the frequency scan, set up the time-corrected gain circuit, signal averaging, pulse cycle count, and diplexer options to acquire optimal echo response.
4. Begin signal collection using the determined system settings.
5. If a defect echo is received (i.e., ahead of the back wall), perform a gated frequency scan of the back wall and new echo by setting appropriate gate positions.
6. If the echo exhibits maximal response at other than the predetermined scanning frequency or frequencies, then recollect a new A-scan at this maximal response for later analysis.
7. Resume inspection of remaining rods using the frequency or frequencies acquired at step 4.

3.2 Embedded system requirements

Since the test method presented above is for configuration of a laboratory-type system, it is more involved than that of a specialized embedded system. The embedded system will simplify several configuration steps such as frequency scanning, optimal cycle count determination, and the setting of the time-corrected gain function. Additionally, the requirements

for detection of nonlinear influences will also be incorporated and require other components of inspection and setup. These might be simple with nonlinear methods such as frequency mixing or harmonic analysis or somewhat more involved for methods such as impact modulation.

Migration from the laboratory system to an embedded system is needed for several reasons. In addition to simplicity of setup and operation as mentioned above, the portability and cost can further be improved. If permanent on-site, long-term monitoring is desired, the system size and cost parameters become even more critical. Initially, the option of modifying or reconfiguring existing commercial NDT hardware was considered as it would provide the most cost-effective transition strategy. The systems investigated for this purpose included sonar, metal inspection, guided-wave pipe systems, and more specialized airborne composite systems. These systems failed to be adaptable for a multitude of reasons.

The general hardware configuration being currently used is a 2 in., 2.25 MHz Accuscan transducer, a Ritec Instruments SNAP system with linear diplexer and fast recovery preamplifier, along with a high end oscilloscope, and a function generator driving a time-corrected gain circuit. Better or equal performance using a reduced hardware footprint is the transition goal (Figure 20). An initial step will be to integrate the fast-recovery preamplifier with the time-corrected gain circuit and its driving function generator. The second phase will be to transition from the high-end digital storage oscilloscope to either a notebook or *computer on a stick* interfacing a high-performance, low-cost digitizer such as the PicoScope 5244B. The final stage will be focused on replacement of the Ritec system's pulse generation and, depending on their necessity, its heterodyne detection and nonlinear measurement capabilities. Texas Instruments is an example of a vendor which supplies numerous specialized integrated circuits that are used for developers of embedded ultrasonic systems and whose component offerings may be useful in this hardware transition phase.

3.3 Optimization of system

Even with site-specific, low-loss-mode propagation modes, detection of reflected echoes through hundreds of feet of embedded rod is very system demanding and requires exploitation of multiple enabling methods and technologies. A table is provided below which describes various mechanisms in the current ERDC system and their contribution toward improved system performance.

Figure 20. Migration of system from laboratory equipment to portable system.

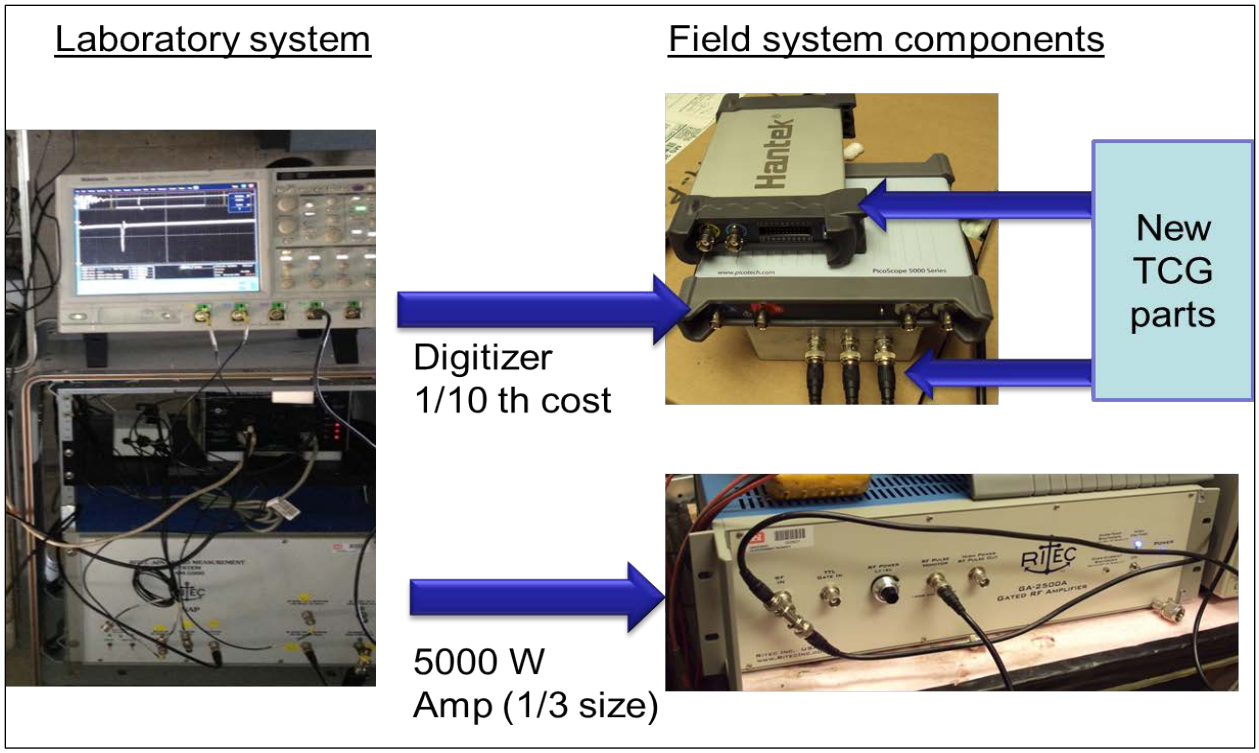

Table 2. Assemblies contained in present system.

System Component or Method	Benefit or Contribution
Signal averaging	Reduction in nonstationary noise which is largely due to high system gain (~100 db)
Narrowband signal (70-200 cycles)	Concentrates energy in desired propagation mode and improves response of PZT transducer
High-output/sensitivity PZT or PMN-PT	Maximum performance transduction technologies
Time-corrected gain amplifier with nonlinear ramp	Extends detectability to entire rod length while still allowing high gain and high pulser voltages
Large-area/medium damped transducer	Maintains high output levels and sensitivity while eliminating undesired in-transducer reverberations experienced with low-damped (high response) transducers
High power pulser (5,000 watts)	Stimulates transducer with maximum allowable signal before transducer failure levels
Superhetrodyne phase detector	Improved detection of narrowband signal amplitude and phase information in the presence of stationary noise
Very fast recovery preamplifier	Prevents preamplifier saturation of diplexer output from masking rod defects that may be located near the transducer
High-pass and low-pass filtering	Reduction of unwanted noise sources
Tunable diplexer	Optimizes pitch catch operation and takes advantage of limited injection area
On-site, Pre-inspection scanning with gated narrowband signals	Allows determination of optimum low-loss inspection modes at each site

Because the current system can acquire over 600 ft of propagation length, scenarios such as shorter and larger diameter rods allow multiple backwall echoes to be acquired. This is a desirable configuration as it allows improved confidence with the second and even third occurrence of any defect echoes. It should be noted that some small spectral change occurs due to the influence of the transducer absorbing and therefore slightly changing the spectral content of what is reverberating in the rod. This effect is constant and only changes the received spectrum between the first and second reverberation.

4 Rod Coupling

In the development of an ultrasonic guided-wave testing method for posttension trunnion anchor rods, it was found that optimum coupling occurs when a large-diameter transducer was placed on the flat end of the anchor rod. Significant efforts were made to develop a transducer and coupling process for the curved sides of the rod as it was known early on that the exposed rod end is frequently field cut, with a cutting torch, after tensioning. This torch-cutting process produces a surface whose roughness is not suitable for transducer coupling. Figure 21 shows a group of trunnion anchor rods that have been cut using a torch.

Figure 21. Torch-cut rod ends.

Because the low-loss guided-wave frequencies that reflect from the distant end of the rod do not couple efficiently to the outer curved trunnion rod surface, it was not possible to develop a transducer operating in this mode. Efforts were also made to exploit ultrasonic mode conversions occurring upon reflection at the exposed end. Reception of mode-converted energy

near the rod end did not produce sufficient signal levels on long, embedded test-bed rods. As inspection frequency and surface roughness increase, coupling loss becomes greater due to decreased contact area and destructive phase interference. To inject the necessary high-frequency ultrasonic energy into the test piece, the contact surface must be made relatively smooth and/or an improved coupling/transduction method must be found.

4.1 Saw cutting of rod ends

The older and more common method of holding the trunnion anchor rod's tension at the exposed bulkhead is by means of compression-loaded wedge assemblies. These vary in design, but the "Howlett grip nut" type is one of the more commonly encountered versions. Due to the nature of this compression approach and their occasional slippage, any method to flatten or machine the rod end should be either gentle or automated in nature. Both approaches have been investigated here.

A portable bandsaw provides a means of cutting a nearly flat and orthogonal surface with minimal vibration and torque being imposed on the grip assembly. Figure 22 shows a representative portable band saw suitable for field cutting exposed trunnion anchor rod ends. Proper selection of blade teeth geometries, blade construction materials, blade tension, and feed rate will improve both the life of the blade and quality of the cut. In order to maintain a good orthogonal cut, it is helpful to use a guide such as a band of wide tape or a mechanical collar around the rod to provide a reference edge where the cutoff plane should occur.

Figure 22. A portable band saw used to cut ends of rods.

With the portable bandsaw, some slight scalloping in the direction of the blade's cut direction has been observed. Increasing blade tension and decreasing feed rate should help minimize occurrence of this effect. It is difficult to put a definitive number on the time required to perform a cut, as faster cuts can be made at the cost of cut quality and blade life. Approximately 5 minutes is a nominal time to cut with reasonable quality a 1.25 in. diameter rod.

4.2 Grinding

Angle-type hand grinders were evaluated for their capability to smooth a rough rod surface and produce a suitable flat and orthogonal surface. While suitable in terms of speed, hand control of the grinder tended to produce beveled edges, and non-orthogonal surfaces. The vibration and torque appeared to be slightly higher than the portable band saw as the portable band saw provides a reaction surface which opposes the force by which the rod is pulled in cutting. Grinder wheel selection and condition were found to have a very significant influence on the final result. Thin cutoff wheels would flex and produce curved surfaces. Sandpaper, flapper-type wheels caused rounded and beveled edges. Thick abrasive grinding disc would wear faster at their outer surface which then transferred this profile into the rod end. The best disc performance was observed from ¼ in. fibrous grinding disc as shown in Figure 23. While angle grinders produced quick results in terms of material removal, the quality of the finish was less consistent than with the portable band saw.

Figure 23. Angle grinder disc producing best results for rod finishing.

4.3 Coupling to rough surfaces

Ultrasonic coupling performance is determined by many factors. If a test surface is relatively smooth, a thin film of water or petroleum grease is often used to carry the ultrasonic energy from the transducer face into the test object. If this layer of couplant can be kept thin compared to the wavelength of the ultrasonic energy, then acoustical mismatch between the transducer, couplant, and test object can be ignored. Couplants like water and grease have relatively slow acoustical velocities (less than a tenth that of steel). This slow wave speed makes a high-frequency ultrasonic wavelength in these materials very short and creates close spacing of the one-half and one-quarter wavelength coupling. With the speed of sound in water at 1,500 ft/sec and an inspection frequency of 2 MHz, the half wavelength distance will be 0.014763 in.

$$R = \left(\frac{Z_2 - Z_1}{Z_2 + Z_1} \right)^2 \tag{1}$$

The half-wavelength distance corresponds to 180 degrees out-of-phase destructive interference at the injection point. In addition to destructive interference, the increased surface roughness creates a thicker layer of coupling material which creates acoustical mismatch and scattering according to Snell's law. Couplants like quick-set epoxy provide good coupling but are logistically time consuming and typically will not raise the acoustical impedance much beyond approximately 3 megarayls. When observing only reflection loss at normal surfaces for steel with an acoustical impedance of approximately 45 megarayls, there is a reflection coefficient approximately 76% between the epoxy and steel and approximately 70% between the transducer and grease. Since energy has to travel through the couplant in both transmission and reception, the round trips result in less than 4% efficiency for the ideal planar case (i.e., no destructive interference taken into account). This means that for practical testing, either the surface has to be smoother or an alternative coupling material has to be used. Getting an orthogonal and relatively flat surface proves to be problematic even when using the aforementioned off-the-shelf cutting and grinding tools. Several practical solutions are presented in the sections below.

4.3.1 Description of an ideal couplant

Transitions in mechanical impedance determine relative reflection and refraction coefficients while acoustical velocity and path length drive destructive phase interactions in the test specimen. In general, there is a need to increase both mechanical impedance and acoustical wave speed in the couplant to reduce the coupling losses (Table 3). In a planar case, the ideal acoustical coupling layer between the transducer would be an odd increment of a quarter of a wavelength in thickness and have an acoustical impedance that is the geometric mean between the rod and transducer. The wear plate on the Accuscan faceplates is one-quarter wavelength of Alumina material which has an acoustical impedance of 40.6 MRayls, and the steel's acoustical impedance is approximately 45 MRayls. The optimum transition material would have an impedance of 42.4 MRayls. To minimize destructive reverberations and phase in the couplant, it is desirable have a couplant with an acoustical velocity aproximately 5900 meters per second (m/sec). These desired mechanical properties are far from what can be offered by standard ultrasonic couplants.

Table 3. Typical couplant materials acoustic characteristics.

Material	Vl	ρ	Z
Alumina	10520	3.86	40.6
Steel	5900	7.8	45.0
Epotek 301	2640	1.08	2.85
Tungsten	5200	19.4	101.0
Gallium	2740	5.9	16.3
Field's metal	2617	7.8	20.6

4.3.2 Low melting point metals for ultrasonic coupling

In searching for candidate coupling materials, a group of nontoxic, low-melting-point metals and metal alloys were found. The concept put forth was that a cast of the imperfect rod end can be made while this metal is in its liquid state; upon re-solidification, the solid ingot can be grease coupled between the imperfect rod and flat-faced transducer to achieve improved high-frequency ultrasonic coupling. Gallium was the first material investigated as a couplant in this class. This is a nonstandard use of these materials, and very little acoustical information has been found in the literature regarding this novel application. A proof-of-concept with gallium on a rough-cut rod sample revealed losses on the order of 60%. Since three

or four reverberations are usually achievable on 60 ft rods of 1.25 in. diameter with flat ends, this level of efficiency validated the application for ultrasonic guided-wave coupling to rough-ended trunnion anchor rods. Additional investigations were continued in order to improve on this approach. Gallium has a melting point that is approximately 100 °F. High ambient temperatures, melting under contact with human skin, and slow transitions from liquid back to solid condition became obvious problems with using gallium.

4.3.3 Field's metal

Field's metal, or Field's alloy, is a fusible alloy that becomes liquid at approximately 62 °C (144 °F). This higher melting point results in less unintentional melting and quicker resolidification after casting. Field's metal is an eutectic alloy of bismuth (Bi), indium (In), and tin (Sn), with the following percentages by weight: 32.5% Bi, 51% In, 16.5% Sn. Most commonly this material is used for die casting and rapid prototyping, which indicates that it has low viscosity when melted and low volume change during state transitions. Unlike Rose's metal and Wood's metal, Field's metal is considered nontoxic. At the time of this report's writing, Field's metal cost was approximately $300 to $1000 per pound depending on the source. As this material can be melted and recast repeatedly and only a small volume is required per rod casting, this price is not seen as prohibitive. Notably, a few lower-cost and still nontoxic alternatives exist such as alloys of 62.5% Bi, 37.5% Sn (5 parts Bi, 3 parts Sn). This alloy is cheaper than Field's metal but melts at 202 °F.

Lab experiments were performed on a cast cylindrical sample approximately 2 in. long to determine the relevant mechanical properties of this material. Through-transmission measurements were performed with shear-wave transducers to produce the waveforms shown in Figure 24.

The results from these measurements indicate a compressional wave speed of 2617 m/sec and a shear-wave speed of 1065 m/sec. Using a density of 7.9 grams per cubic centimeter (g/cm^3), the resulting acoustical impedance is calculated to be 20.6 MRayls. The tensile strength is approximately 33 MPa, the Young's modulus 25 GPa, and the value of Poisons ratio is approximately 0.4.

Figure 24. Waveforms of Fields metal through-transmissions.

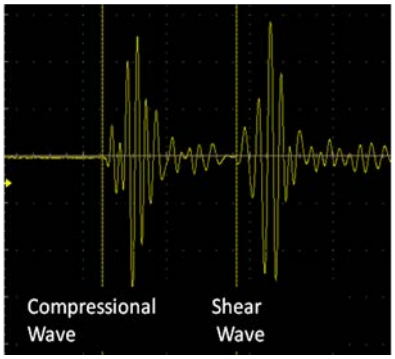

A prototype casting device was developed to test the Field's metal ingot coupling performance across a variety of conditions on actual full-length, grease-embedded trunnion anchor rods in the ERDC test bed. Unlike the initial proof-of-concept, which was cast on a small vertical rod so that gravity would form the flat backing, this system required the melted Field's metal to fill a volume between the rod face and flat backing that the transducer would couple to. Figure 25 below shows the prototype device. The melted/liquid Field's metal is placed in the large syringe and then pressurized with the plunger until the casting volume is filled and the liquid material exits the small vent hole at the top of the casting volume.

Figure 25. Casting fixture.

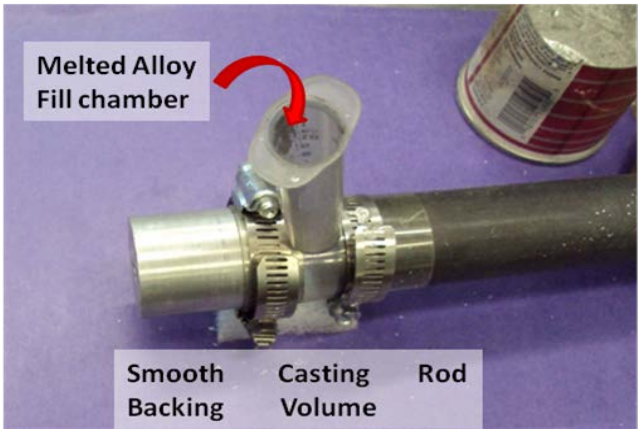

Typically, in 1 to 2 minutes, the Field's metal has set, and the casting apparatus can be removed. This prototype design allows casting on horizontal or inclined bars and variability in casting thickness. Portable propane stoves such as those used in backpacking can be utilized as an easy field system for heating the Field's metal to its 140 °F melting point. An example of cast ingots is shown in Figure 26. These castings do not form an

adhesive bond with the rod or casting apparatus and can be easily removed once solidified. Due to this lack of adhesion, a small thin layer of grease is applied to each side to form good ultrasonic coupling. According to theory, the calculated loss due to impedance mismatch between the transducer faceplate and Field's metal is 10% reflected or 90% transmitted. Likewise, the energy in the Field's metal traveling into the anchor rod undergoes 13.8% reflection or 86.2% transmission efficiency. Combining these two layers, the overall transmitted and reflected energy through the Field's metal is 77.6% and 22.4%, respectively. Because the ultrasonic energy must travel through these layers twice (in transmission and reception), the overall loss from reflections into and out of the coupling medium is approximately 40% from the transducer into the rod and back. Mode-conversion losses at the end of the rod can be conservatively approximated to be less than 5%.

Figure 26. Rod end castings.

4.3.4 Field's metal coupling as a function of surface condition

An investigation was performed to study the effect of rod's end surface condition on guided-wave inspection frequencies and attenuation. The end of the rod was varied from a rough replication of a torch-cut condition to flat. For attenuation and spectral response, these conditions were referenced to the flat rod coupled directly to the transducer (Figure 27). Two rough conditions were investigated; these included a rough rod-end condition with deep-cut grooves approximately 1/16 in. deep and a second rough condition where a 1/8 in. sloped cut was superimposed on 1/16 in. groove cuts. These two rough end conditions were created to mimic field torch-cut rod ends. A grinder was used to perform coarse flattening of the two rough conditions so that the depth of the roughness was approximately one-half

its original condition. This grinding action corresponded to 2 to 3 minutes of grinding time. These samples were labeled as the two medium conditions. Last, a flat sample was prepared where the portable band saw was used to cut off the rough section of the rod and leave a nearly flat and and perpendicular end. In prior work as described in section 2.3.3 of this report, reverberations were used to estimate guided-wave acoustical propagation loss rates for various diameter rods. A similar process of reverberation measurements and comparisons were used to evaluate Field's metal coupling performance to various surface conditions.

Figure 27. Flat Field's metal coupling piece amplitude of first two echoes used to estimate coupling efficiency.

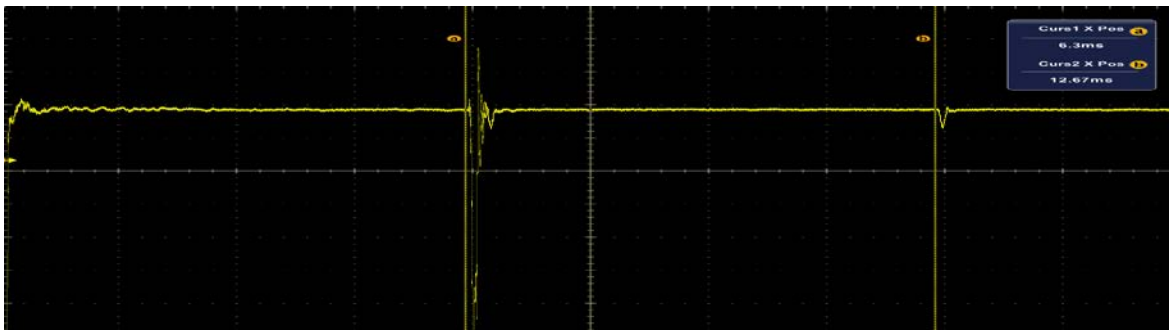

Five surface conditions were investigated. These represented two rough conditions, including two rough-cut rod ends, one with an overall angle and one relatively orthogonal, and two medium conditions where a short grinding operation of several minutes was used to flatten the high spots on the rod, and last, a flat condition from cutting with a portable band saw. Figure 28 shows two cast ingots from the medium and rough condition.

Figure 28. Medium and rough surface Field's metal castings.

Figures 29 and 30 show the attenuation results from various surface condition comparisons in decibels and percentages. These results are normalized with respect to the transducer coupled on a flat rod end. This process removes the material attenuation and provides a frame of reference with respect to an ideal condition.

Figure 29. Field's metal coupling performance to various surface conditions (dB).

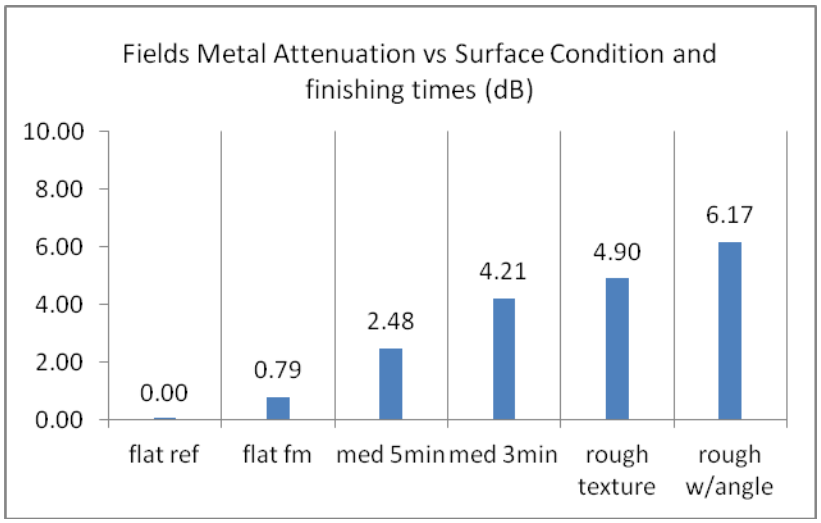

Figure 30. Field's metal coupling performance to various surface conditions in percentages.

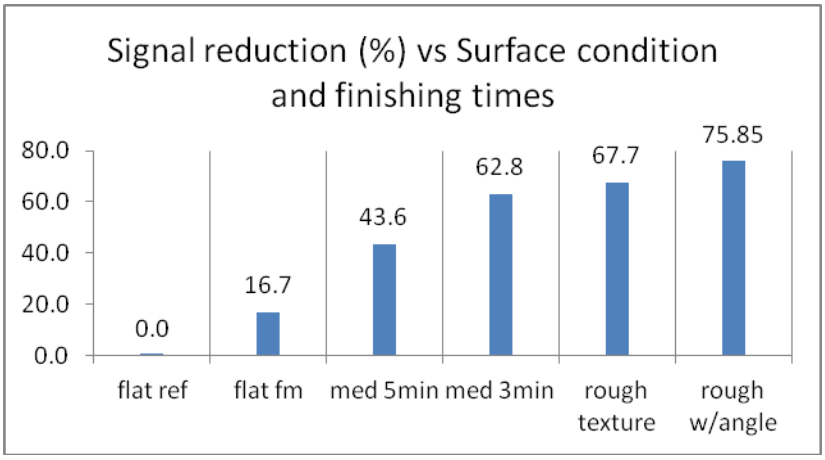

These findings indicate, as expected, that the Field's metal coupling performance degrades with surface roughness due to destructive phase interactions at the Field's metal/rod interface. Based on these numbers, it is still possible to receive backwall reflections on most rough-cut rod surfaces. Using a system dynamic range of 108 dB and the .2 and .6 dB loss rates for 1.25 and 1.125 in. diameter rods, respectively, Table 4 was

generated to show the effective rod lengths in feet that can be inspected as a function of surface roughness.

Table 4. Rod lengths in feet that can be inspected as a function of surface roughness.

rod diameter	ref flat	flat FM	medium	medium	rough	rough/angle		attenuation rate	
1.25 inch	275	273	269	264	263	260		0.2	
1.125 inch	92	91	90	88	88	87		0.6	

Figure 31 shows the fourth echo received with the flat Field's metal ingot; this corresponds to 480 ft of propagation in embedded 1.25 in. rod at a test frequency of 2.39 MHz.

Figure 31. Long-distance propagation verified through flat ingot of Field's metal.

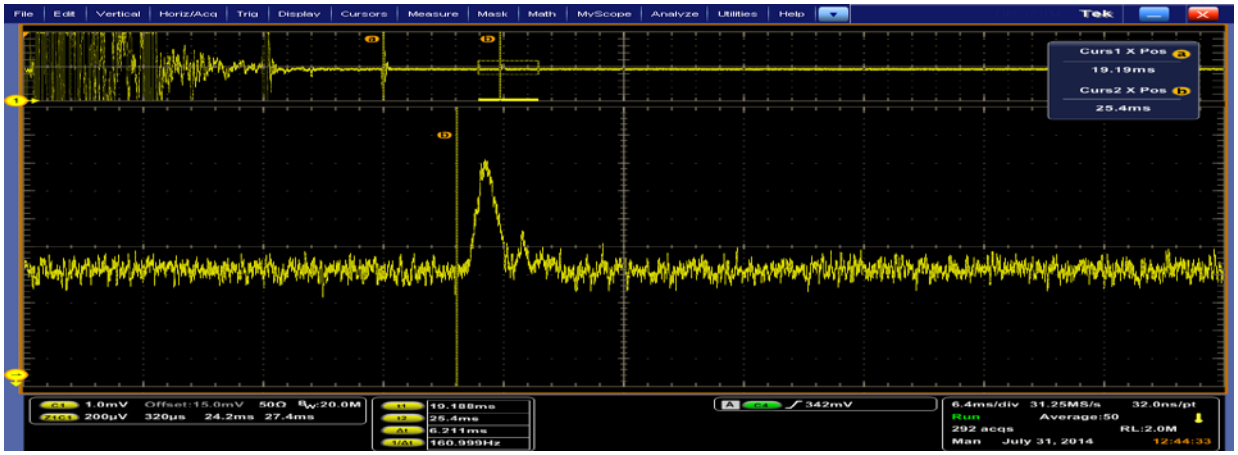

4.3.5 Guided-wave spectrum and surface condition

In previous trunnion anchor rod testing with guided waves, it was found that the spectral response of the higher-order guided-wave modes did not change significantly from rod to rod for rods of a given size. Because surface roughness creates frequency-dependent scattering, the previously mentioned surface roughness variations were investigated with spectral guided-wave scans. As expected, for the rougher surface conditions, more attenuation and scattering were observed. For the flat rod coupled with a Field's metal casting, the ideal inspection frequency is unchanged when compared to a rod directly coupled with the transducer (shown in Figure 32, top). For the medium and rough conditions (Figure 32, middle and bottom, respectively) the ideal low-loss higher-order modes can be seen moving towards the lower-order guided-wave modes which are correspondingly lower in frequency.

Figure 32. Spectral frequency shift as surface roughness increases.

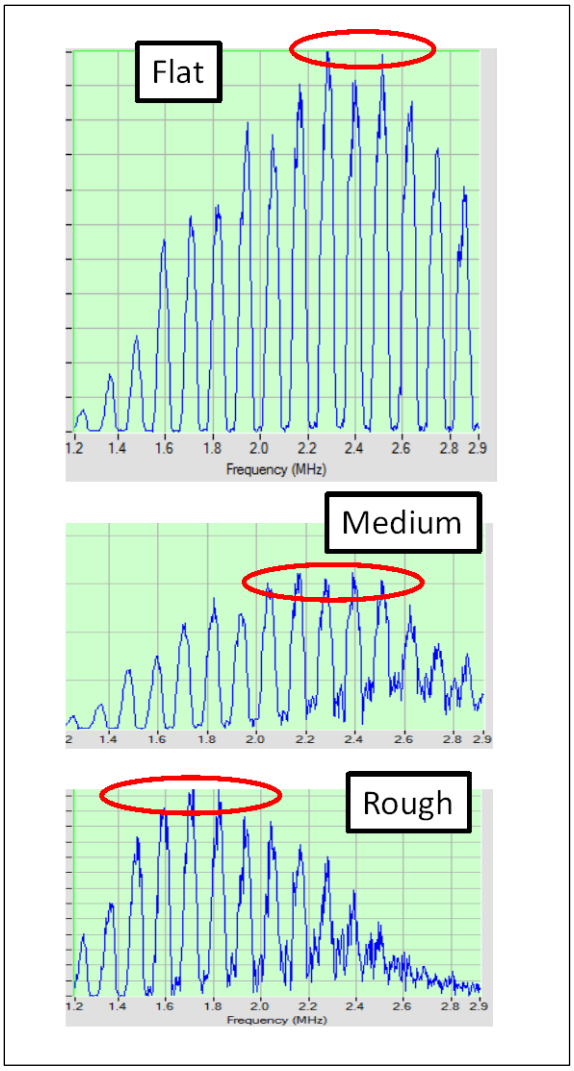

This leads to an expected test-method modification where either a more robust lower-order mode is selected or more ideally, a quick scan is performed on each rod to verify and determine the ideal propagation frequency for that particular rod. This second option would minimally add a few minutes of testing to the inspection time required for each rod.

4.3.6 Recommendations for Field's metal-based coupling

In order to optimally couple a flat transducer face to a rod end, the rod end should be cut orthogonally and made flat. While polished surface is not necessary, flatness has a significant influence. Grease can fill any air gaps, but surface variation on the order of .01 in. begins to create losses due to scattering and destructive phase interactions. It is relatively easy to create

somewhat flat surfaces using grinders and portable band saws, but it is very difficult to make those surfaces perfectly flat. For large diameter rods 1.25 in. and above, Field's metal coupling should allow the reception of multiple reverberated echoes over practical in-situ rod lengths. For more attenuative cases such as long small-diameter rods, a light-grinding with an angle grinder, or more ideally, rough end removal with a portable bandsaw, prior to Field's metal coupling would be preferred. Table 4 provides guidance on testable lengths and can be used to determine what needs to be done for the given rod surface condition, length, and diameter.

4.4 Proof of concept for automated end finishing

In the following, an alternative finishing process is described. A proof-of-concept investigation was performed to explore an improved rod finishing process. The intent of this process is to ultimately provide for automated and consistent finishing of rod ends that are orthogonal and flat without a need for Field's metal coupling. A cup grinding method is conceptualized for eventual implementation with a robotic/automated grinding accessory. A three- or four-jawed chuck would ultimately serve to both hold the finishing apparatus and maintain orthogonality with the rod. The automatic end finishing actuators and rotational grinding motor would be attached to a through-hole chuck as shown in Figure 33.

Figure 33. Through-hole chuck that would serve as a rod-mounted platform for finishing.

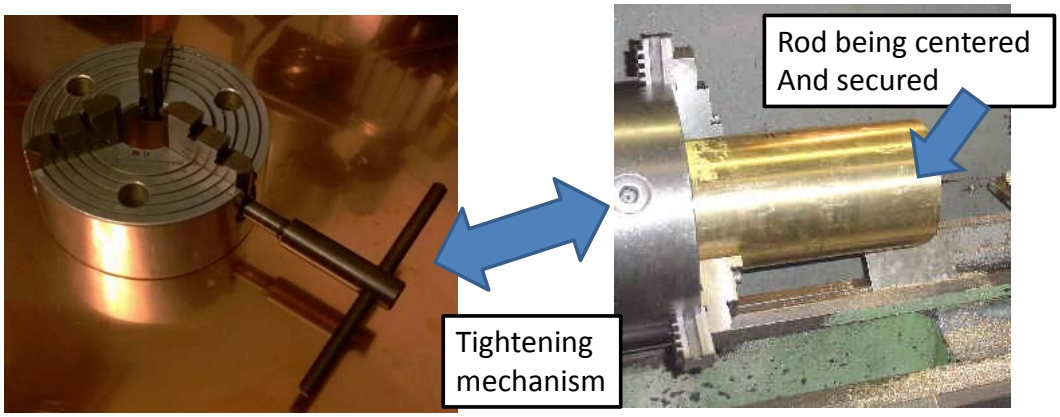

A cup grinding mechanism (conceptionalized) is shown in Figure 34. The advantage of this stile stone and finishing action is that it promotes even grinding-stone wear due to high points on the rod being constantly exposed to different radial positions on the stone. This helps the stone last longer and provides a flatter finish.

Figure 34. Side view and end view of cone grinding process for end-of-rod finishing.

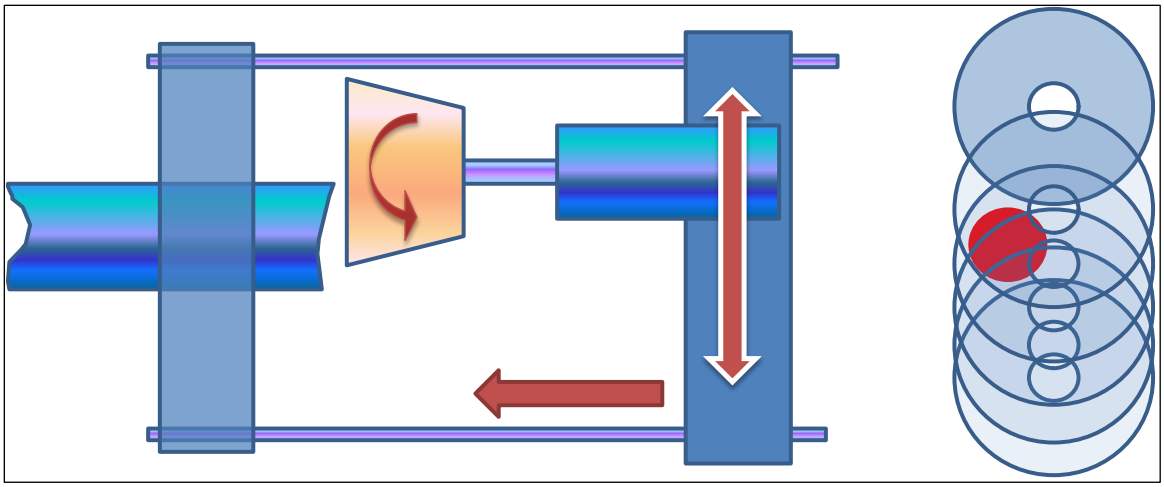

Example pictures of grinding cups are shown in Figure 35 (left), and Figure 35 (right) shows the grinding cup used in this investigation prior to grinding a rough ended rod. The mechanism in this experiment was swung in a rotational arch instead of a linear path.

Figure 35. Example grinding cups (left); cup and rod prior to grinding (right).

Figure 36 shows the second-pass results and final surface finish.

An automated rod finishing system is proposed where a self-centering and aligning through-hole chuck would be used to secure a cup grinding apparatus to the rough-ended rod. After setting the beginning and ending grinding depth, an operator would turn the device on, and the remaining movements would be automated. The proof-of-concept effort showed that this approach will produce smooth and orthogonal finishes on rough-ended rods.

Figure 36. Second-pass grinding (left); finished surface (center); resulting flatness (right).

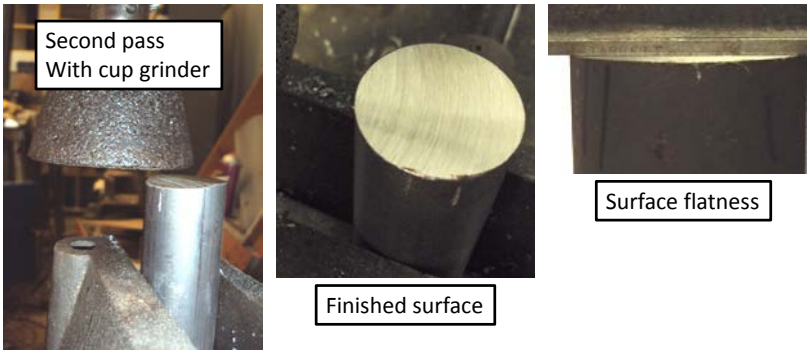

5 PMN-PT Transducers

Guided-wave testing of embedded trunnion anchor rods can in some cases push the limits of conventional high power/high sensitivity PZT based piezoceramics. PMN-PT-based material represents a new and emerging piezoelectric crystal with potential performance increases up to five times those of previously available piezoelectrics. While this new material has not yet made its way into commercially available transducers, it is available as a raw piezoelectric crystal. Some of these crystals were procured in Fiscal Year 14 to investigate development of an improved transducer for trunnion anchor rod inspection. At the time of procurement, elements of 0.853 in. diameter were available. While this size element is smaller than what would have been ideally preferred, it still allows for relative performance evaluation with PZT transducers. Because of their low production volumes, these elements are still relatively expensive. In order to best investigate this material, a transducer housing system was developed to allow various backing materials to be inserted for testing. Figure 37 shows the various hardware components in the constructed transducer. Backing materials with various components and combinations of components were investigated; these components include ground cork, tungsten, and assorted epoxies. By varying the backing material's acoustical impedance, the quality factor (or bandwidth) of the transducer can also be varied.

Figure 37. Components in PMN-PT transducer with interchangeable backing material.

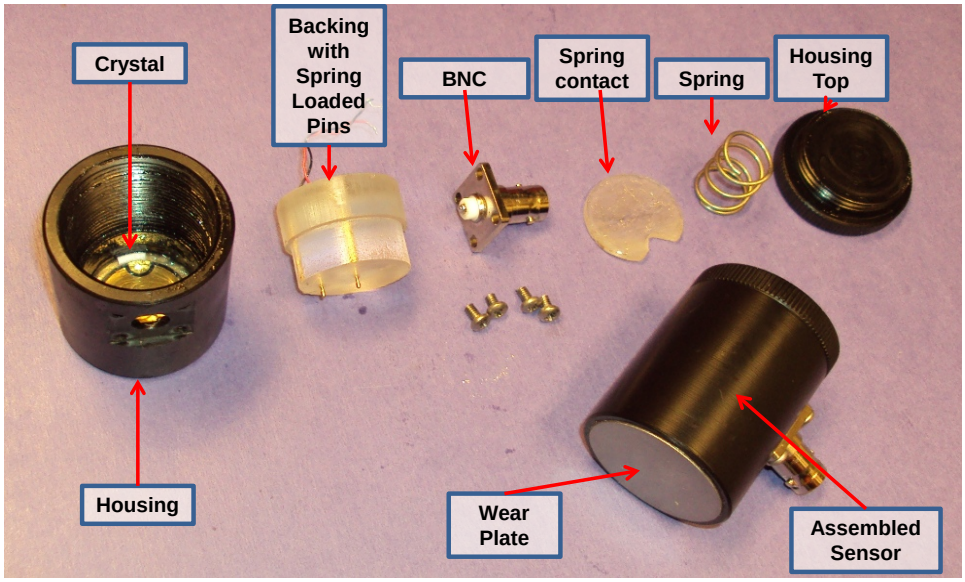

The PMN-PT material investigations are still underway, and backing materials and transducer construction variations are still being explored. In the initial design, a limitation in transducer bandwidth is being observed. Figure 38 shows the spectral guided-wave scan of the embedded rod. Typically for the Accuscan low-damped transducer, the guided-wave modes extend from 1.4 MHz to over 3 MHz; it is evident in Figure 38 that a much smaller spectral range is resulting from the PMN-PT material.

Figure 38. Guided-wave rod scan with PMN-PT showing limited bandwidth.

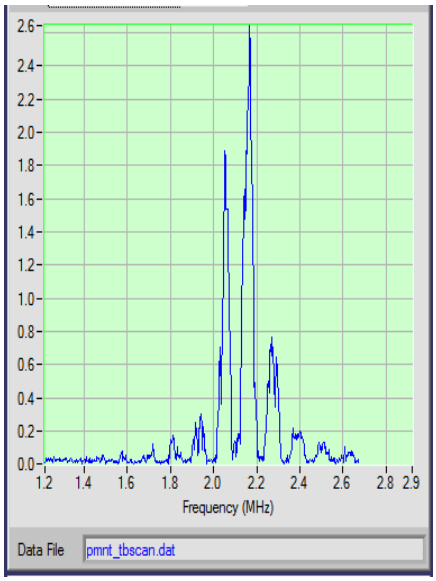

Figure 39 shows a clear second echo from the PMN-PT transducer on a grease-embedded 1.25 in. rod corresponding to 240 ft of propagation.

Figure 39. Second and third reflections on embedded rod from PMN-PT transducer.

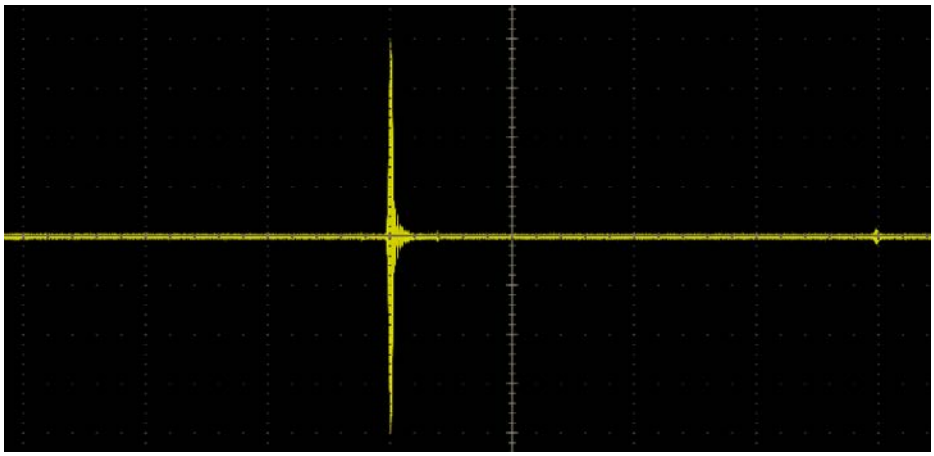

In Figure 40, the same pulse is compared to a reflection at the same inspection frequency with the Olympus Accuscan transducer.

Figure 40. Larger second echo from PMN-PT vs. PZT transducer.

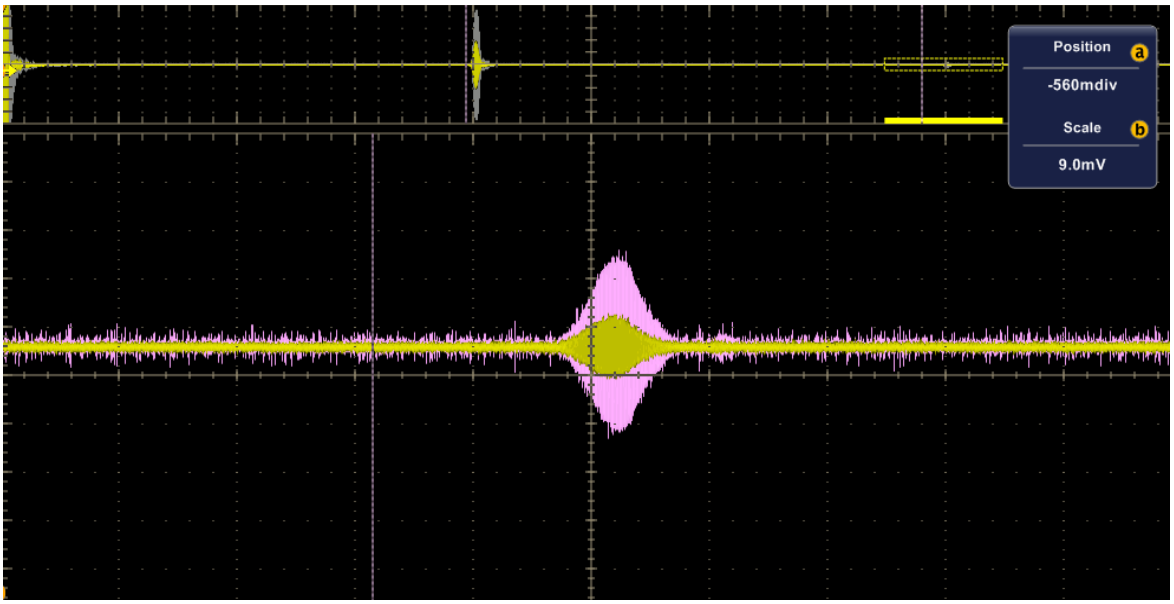

It is important to note that the Olympus crystal is 1.5 in. in diameter, which correlates to a crystal diameter 3.5 times that of the PMN-PT material being tested. This bigger reflection using a significantly smaller area crystal indicates the high-performance capability stated for PMN-PT materials. Investigations are continuing to improve the PMN-PT transducer bandwidth response.

6 Conclusions and Recommendations

The use of ultrasonic guided waves to detect cracks in trunnion rod has shown to be an effective means of detecting cracks in trunnion rods. The presence of a *soft* corrosion product in the observed crack areas provides an acoustical reflector suitable for defect detection. In mock-up, test-bed investigations, notches as shallow as 0.1 in. were detected at realistic distances in embedded rods. This research has quantified the influence of site variables such as rod diameter, end conditions, tension, etc., on the performance of higher-order longitudinal guided waves. Furthermore, optimized system parameters and a deployment test method have been defined such that this technology is ready for transition into a turnkey portable field system. This field system is currently under development, and once deployed at demonstration sites, will provide much-needed condition data and monitoring records for embedded trunnion anchor rods.

References

Beard, M. D., M. J. S. Lowe, and P. Cawley. 2003. Ultrasonic guided waves for inspection of grouted tendons and bolts. In *Journal of Materials in Civil Engineering*, 212–218. London SWY 2BX, UK: Department of Mechanical Engineering, Imperial College.

Beard M. D., M. J. S. Lowe. 2003. *Non-destructive testing of rock bolts using guided ultrasonic waves*. London SWY 2BX, UK: Department of Mechanical Engineering, Imperial College.

Buck, O., W. L. Morris, and J. N. Richardson. 1978**.** Acoustic harmonic generation at unbounded interfaces and fatigue cracks. *Applied Physics Letters* 33(5): 371–373.

Cesare, M. A., and J. D. Holt. 2012. *Inspection of trunnion rods at Greenup Dam*. Raleigh, NC: FDH Engineering Inc.

Ekimov, A. E., I. Didenkulov, and V. Kazakov. 1999. Modulation of torsional waves in a rod with cracks. *Journal of the Acoustical Society of America* 106(3): 1289.

Evans, J., R. Haskins, J. Padula, and J. Hite. 2013. *Trunnion rods activities for microcrack detection*. ERDC/CHL CHETN-IX-32. Vicksburg, MS: U.S. Army Engineer Research and Development Center. http://chl.erdc.usace.army.mil/chetn

Evans, J., and R. W. Haskins. 2013a. *Guided-wave testing of trunnion rods at Greenup Dam, Kentucky*. ERDC/CHL CHETN-IX-35. Vicksburg, MS: U.S. Army Engineer Research and Development Center. http://chl.erdc.usace.army.mil/chetn

Evans, J. A., and R. Haskins. 2013b. Development of a guided-wave technology capable of the detection of open cracks and microcracks in embedded trunnion anchor rods. ERDC/CHL CHETN-IX-36. Vicksburg, MS: U.S. Army Engineer Research and Development Center. http://chl.erdc.usace.army.mil/chetn

He, C., J. K. Van Velsor, C. M. Lee, and J. L. Rose. 2006. Health monitoring of rock bolts using ultrasonic guided waves. In *Review of Quantitative Nondestructive Evaluation Vol. 25*, ed. D. O. Thompson and D. E. Chimenti. College Park, MD: American Institute of Physics.

Headquarters, U.S. Army Corps of Engineers (HQ USACE). 2000. *Engineering and design–Design of spillway tainter gates.* EM 1110-2-2702. Washington DC: Department of the Army, U. S. Army Corps of Engineers.

Guyer, R. A., and P. A. Johnson. 1999. The astonishing case of mesoscopic nonlinearity. *Physics Today*.

Jhang, K-Y. 2000. *Applications of non-linear ultrasonic to the NDE of material degradations.* Seoul, Korea: Hanyang University, School of Mechanical Engineering.

Johnson, P. A. 1999. The new wave in acoustic testing. *Materials World, the Journal of the Institute of Materials* 7: 544–546.

Johnson, P. A. and A. M. Sutin. 2005. Nonlinear elastic wave NDE I: Nonlinear resonant ultrasound spectroscopy and slow dynamics diagnostics. In *Review of Quantitative Nondestructive Evaluation Vol. 24*, ed. D. O. Thompson and D. E. Chimenti. New York: American Institute of Physics.

Korotkov A. S., and Sutin A. M. 1994. Modulation of ultrasound by vibrations in metal constructions with cracks. *Acoustics Letters* 18: 59–62.

Kazakov, V. V., A. M. Sutin, and P. A. Johnson. 2002. Sensitive imaging of an elastic nonlinear wave-scattering source in a solid. *Applied Physics Letters* 81(4): 646–648.

Kazakov, V. V., and P. A. Johnson. 2002. Nonlinear wave modulation imaging. In *Nonlinear Acoustics at the Beginning of the 21st Century*, ed. O. V. Rudenko and O. A. Sapozhnikov, Vol. 2, 763–766.

Luo, J., W. Hackenberger, S. Zhang, and T. R. Shrout. 2009. The progress update of relaxor piezoelectric single crystals. *Ultrasonics Symposium (IUS), 2009 IEEE International*, 20–23 September 2009, ISBN 978-1-4244-4389-5.

Ostrovsky, L. A., and Paul Johnson. 2001. Dynamic nonlinear elasticity in geomaterials In *Rivista Del Nuovo Cimento*, Vol. 24, No. 7.

Pavlakovic, B. N., M. J. S. Lowe, and P. Crawley. 2001. *High-frequency low-loss ultrasonic modes in imbedded bars*. London SWY 2BX, UK: Department of Mechanical Engineering, Imperial College.

Pruell, C., J. Y. Kim, J. Qu, and L. Jacobs. 2009. Evaluation of fatigue damage using nonlinear guided waves. *Smart Materials and Structures* 18: 1–8.

Roach, D. 2007. Improving in-service inspection of composite structures CACRC inspection task group update application of advanced NDI to composite NDI. Commercial Aircraft Composite Repair Committee, Sandia National Labs, Infrastructure Assurance Center & NDI Department, FAA Air Worthiness Assurance Center. http://www.niar.wichita.edu/NIARWorkshops/LinkClick.aspx?fileticket=NgHRjcSrm8s%3D&tabid=110&mid=600

Rose, J. L. 1999. *Ultrasonic waves in solid media*. University Park, PA: Cambridge University Press.

Sun, Z., L. Zhang, J. Rose. 2005. Flexural torsional guided wave mechanics and focusing in pipe. *Journal of Pressure Vessel Technology, ASME* 127: 471.

Sutin A. M., and D. M. Donskoy. 1998. Vibro-acoustic modulation nondestructive evaluation technique. In *Proceedings SPIE*, 3397, Nondestructive Evaluation of Aging Aircraft, Airports and Aerospace Hardware II, 226–237.

Sutin, A. M., and P. A. Johnson . 2005. Nonlinear elastic wave NDE II: Nonlinear wave modulation spectroscopy and nonlinear time reversed acoustics. In *Review of Progress in Quantitative Nondestructive Evaluation, Vol. 24*, 385–392. New York: American Institute of Physics.

Ulrich T. J., P. A. Johnson, A. M. Sutin. 2006. Imaging nonlinear scatterers applying the time reversal mirror. *Journal of the Acoustical Society of America* 119(3): 1514–1518.

Ulrich T. J., A. M. Sutin, and P. A. Johnson. 2007. Imaging and characterizing damage using time reversed acoustics. In *Review of Progress in Quantitative Nondestructive Evaluation, Volume 894*, 650–656.

Ulrich, T. J., A. M. Sutin, R. A. Guyer, and P. A. Johnson. 2008a. Time reversal and nonlinear elastic wave spectroscopy TR NEWS techniques. *International Journal of Non-linear Mechanics* 43: 209–216.

Ulrich, T. J., A. M. Sutin, T. Claytor, P. Papin, P. Y. Le Bas, and J. A. TenCate. 2008b. The time reversed elastic nonlinearity diagnostic applied to evaluation of diffusion bonds. *Applied Physics Letters* 93(15): art. no. 151914.

Van Den Abeele, K., P. A. Johnson, A. M. Sutin. 2000. Nonlinear Elastic Wave Spectroscopy (NEWS) techniques to discern material damage, Part I: Nonlinear wave modulation spectroscopy. *Research in Nondestructive Evaluation* 12(1): 17–30.

Van Den Abeele, K., A. Sutin, J. Carmeliet, and P. A. Johnson. 2001. Micro-damage diagnostics using non-linear elastic wave spectroscopy (NEWS). *Nondestructive Testing and Evaluation International* 34: 239–248.

Yang, H, L. Yu. 2011. *Inspected simulation of port anchor metal rods ultrasonic guide wave based on dispersion characteristics.* Taiyuan, China: National Key Laboratory for Electronic Measurement Technology, North University of China (NUC).

Appendix A: Nonlinear Investigations

A.1 Introduction

Over the last 2 decades, the studies of the application of nonlinear acoustics for crack and defect detection in engineering materials have steadily increased. Numerous experimental and theoretical investigations demonstrated that cracks and other defects in solid structures have strong acoustic nonlinearity, and nonlinear acoustic effect can be used as extremely sensitive tools for NDE.

Different nonlinear effects can be employed in a variety of NDE approaches. There are a number of reviews describing the application of nonlinear acoustic methods in NDE (Guyer and Johnson 1999; Ostrovsky and Johnson 2001; Johnson 1999). The investigation of nonlinear effects includes second and third harmonic generation, modulation of sound by LF vibrations, amplitude-dependent internal friction, and amplitude-dependent resonance frequency shifts.

Historically, the first applications of nonlinear acoustic techniques for material characterization used measurements of the second and higher harmonics generated by the nonlinear distortion of a primarily sinusoidal acoustic wave propagating in a medium with defects. The first test of this method was made as early as 1979 in wave propagation experiments (Buck et al. 1978). This simplest nonlinear method has a serious drawback: generation of high harmonics by power amplifiers and transducers can mask the nonlinearity caused by the material itself. This is likely the reason why nonlinear acoustic methods based on the second harmonics generation and applied for adhesive bond inspection for aircrafts (Roach 2007) report high levels of (false) harmonics even for good-quality bonds.

Later, it was realized that harmonic generation analysis is not the only way (and not always the best way) to implement the effective nonlinear acoustic NDE. Other nonlinear techniques are based on nonlinear observables such as amplitude dependence of the mode resonance peak in a specimen (Van Den Abeele et al. 2001; Johnson and Sutin 2005), on the modulation of HF sound waves by low-frequency vibrations (Korotkov and Sutin 1994; Sutin and Donskoy, 1998; Van Den Abeele et al. 2000; Sutin and Johnson 2005), and on frequency mixing of different frequencies. All these techniques

employ nonlinear wave interactions and/or nonlinear resonances. For the use of resonant modes, these methods need much less acoustic power than the travelling-wave methods.

In these studies, it was found that nonlinear methods are more sensitive to damage-related structural alterations than any known methods based on linear parameters such as wave speed, attenuation, or reflection. Some of these methods allowed finding of a single crack with size much less than applied acoustic wavelengths.

The majority of the nonlinear elastics wave's spectroscopy (NEWS) methods can detect the crack presence but cannot localize cracks. Crack localization can be accomplished by modification of the wave modulation method with an impulse probe wave as described in Kazakov and Johnson (2002). Crack and defect localization can also be accomplished by a recently developed nonlinear time reversal acoustic (NLTRA) method (Ulrich et al. 2008a,b; Ulrich et al. 2006; Ulrich et al. 2007). This method requires expensive and complicated equipment.

The goal of this investigation was the application of nonlinear acoustic NDE for the detection and localization of cracks in long trunnion rods. Posttensioned rods are used to anchor spillway gates and transfer the forces from the reservoir pool through the gates to the spillway structures (HQ USACE 2000). Large tensile loads are applied to these high-strength steel rods to compress the surrounding concrete and prevent it from experiencing excessive tensile forces, which are naturally problematic for concrete. These posttensioned trunnion anchor rods are used extensively for support of tainter gates and are considered the standard for the USACE and other government and nongovernment agencies within the United States and elsewhere. These rods are now experiencing ongoing failures, and nonlinear acoustic methods can be a sensitive tool for early microcracks detection (Evans et al. 2013).

Among the wide choice of the nonlinear NDE methods, the vibro-modulation method (also referred to as NWMS) is one of the simplest for practical applications. The pulse modification of this method was first presented in Kazakov and Sutin (2002) for the case of interaction of tone burst wave with continuous LF vibration. This paper presents the other modification of NWMS based on interaction of tone burst wave with mechanical impulse. This method can provide interaction of HF and LF

acoustic pulses in various areas of the tested rod to indicate the crack localization.

Due to the inherent geometry constraints, the traditional scattering of short wavelengths by defects will, in general, not be successful in detection of a closed microcrack. Nonlinear methods have repeatedly demonstrated their success for characterizing low levels of damage, such as progressive fatigue deterioration and intrinsic material weaknesses using nonlinear acoustics detection methods. Theoretical and experimental research have also addressed key design approaches and explored various embodiments. These include nonlinear impact modulation using different propagation modes and wave types (Eskimov et al. 1999)

A.2 Engineered defects and nonlinear measurement

For nonlinear experimentation, controlled and simulated defects have been pursued. These have included driven-in shims, polished rods in threaded sleeves, and fatigue of aluminum bars from bending. Future efforts will implement a rotational system for propagating a real defect. Loading will, of course, be conservative after quantifying severity. Figure 41 shows some of the simulated crack methods that were used for nonlinear evaluation on rods. These experiments proved successful, with issues regarding transducer coupling nonlinearities coming forward as an important system design consideration.

Figure. 41 Nonlinear crack simulations: two polished ends pulled together (top left), fatigued aluminum (bottom left), nut coupled and shims hammered into a notch (right).

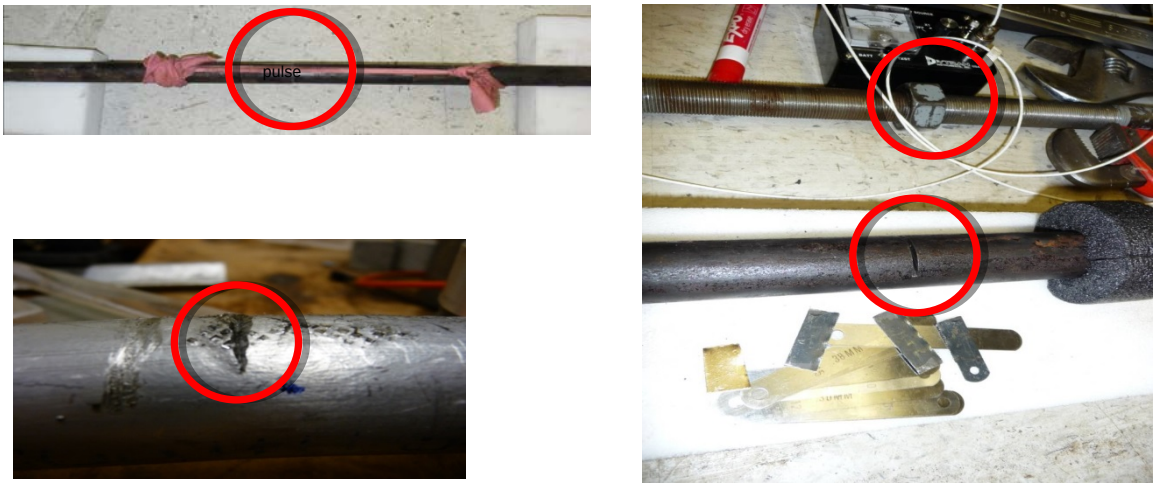

An example nonlinear measurement recently performed at ERDC is shown below in Figure 42. This is an impact-modulated torsional wave to detect a crack simulating defect from hammered-in shims. The modulated sideband frequency is due to nonlinear modulation coming from the shims *chattering*. Ekimov et al. (1999) discuss a similar setup and also characterize dry and lubricated crack influence on nonlinearity.

Figure 42. Nonlinear modulation detected using torsional wave and impact modulation.

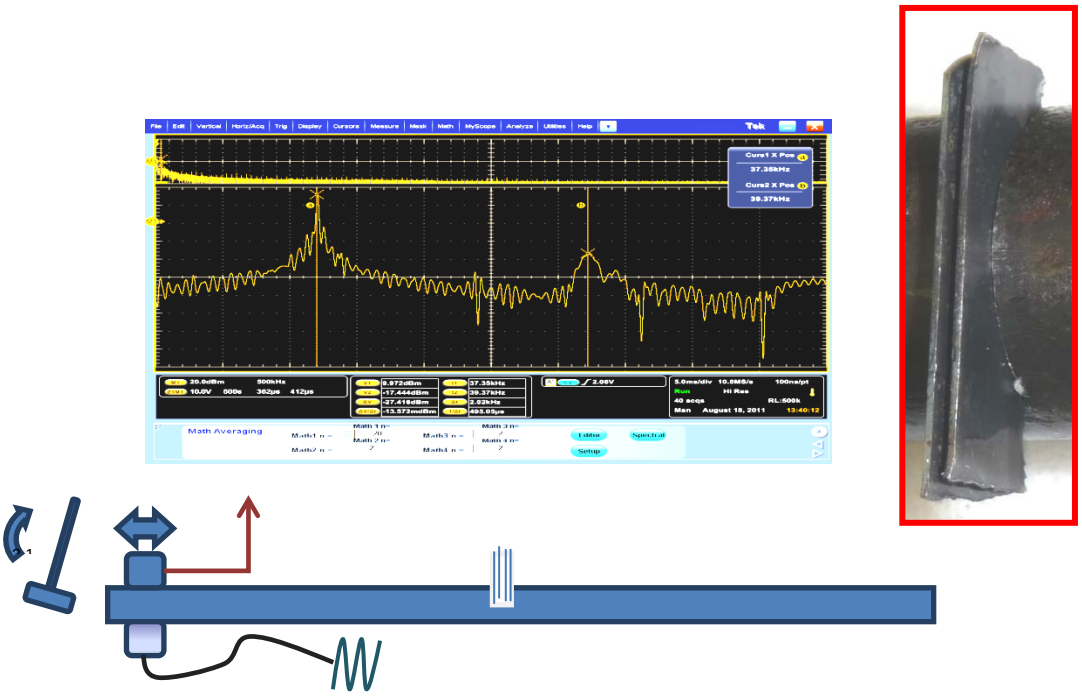

A.3 Phase two nonlinear investigations

Experiments using nonlinear wave modulation spectroscopy (NWMS) were applied to a rod waveguide towards the goal of closed-crack detection. NWMS is one of the simplest methods of nonlinear acoustic NDE based on measurements of the modulation of a HF wave by a LF vibration. Presented here is the modification of the NMWS method based on the modulation of an ultrasonic burst of higher-order longitudinal guided wave by LF pulse produced by a hammer impact. In this method, the variation of time delay between the radiated pulses leads to changes in the downrange area of interaction and therefore allows for crack localization. This feasibility test was conducted for a 60 ft long, steel trunnion rod with an imitated crack. The ultrasound tone-burst longitudinal guided wave with the frequency of approximately 2 MHz was modulated by the longitudinal impulse produced by the hammer impact. Measurements of time delay between the impact

and the received modulated ultrasonic wave allowed for localization of the crack's position

A.3.1 Principles of the modulation of the tone burst with an impulse in long rods

A consideration of how the interaction of HF of tone burst wave with low-frequency impulse can be used for detection of localization of defects in long rods follows. The suggested method can be called impulse-by-impulse modulation (IIM). The most accurate limitation of the interaction area and crack localization can be provided by using interaction of the impulses propagated in opposite directions as shown in Figure 43.

In this setup, it is supposed that the HF probe wave is radiated from the left side of the rod and the LF pulse wave from the right side. The radiation of the HF probe wave is conducted with time delay (τ) regarding the moment of the hammer impact and excitation of the LF wave. The pulses propagated in the opposite directions meet at the distance (x) from the rod end. The meeting point can be found from the expression

$$\frac{L-x}{V_{im}} = \tau + \frac{x}{V_{hf}} \tag{2}$$

where V_{im} is the propagation speed of the impulse wave, V_{hf} is the propagation speed of the HF probe wave, and L is the rod length.

Figure 43. The principles of the IIM method.

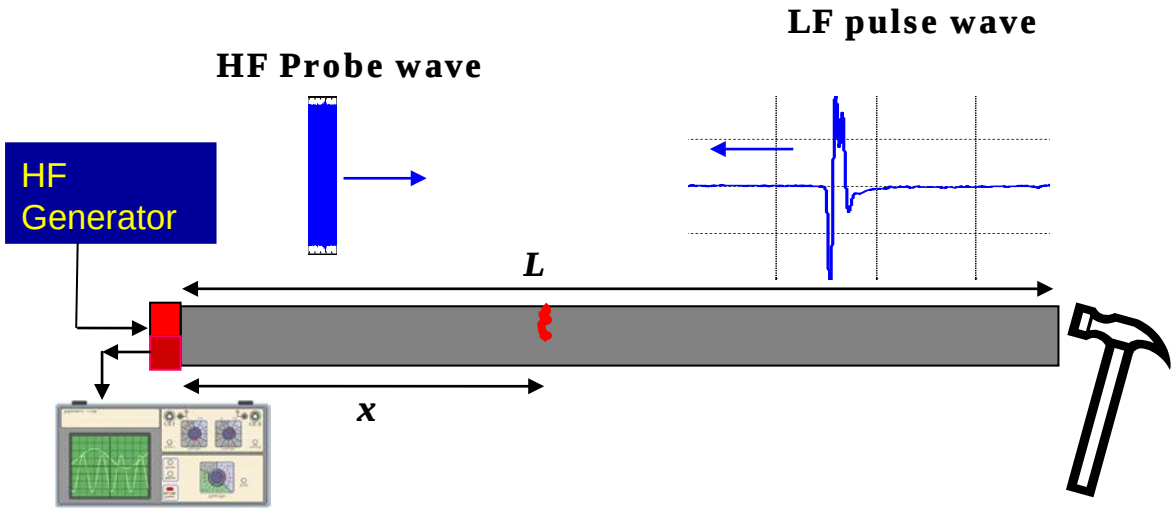

The receiving sensor is attached to the same side as the radiating sensor, and the modulation of the HF pulse can be observed for the pulse reflected from the crack at time $t_1 = 2x/V_{hf}$ or for the pulse reflected from the other side of the rod at time $t_2 = (2L - x)/V_{hf}$. The considered configuration can be used for the method demonstration but not for application for real trunnion rod evaluation because rods in tainter gates have access from one side only. The possible setup for the observation of the two-pulses nonlinear interaction with one-side pulses excitation is shown in Figure 44.

Figure 44. The principles of the IIM method for the same-side excitation.

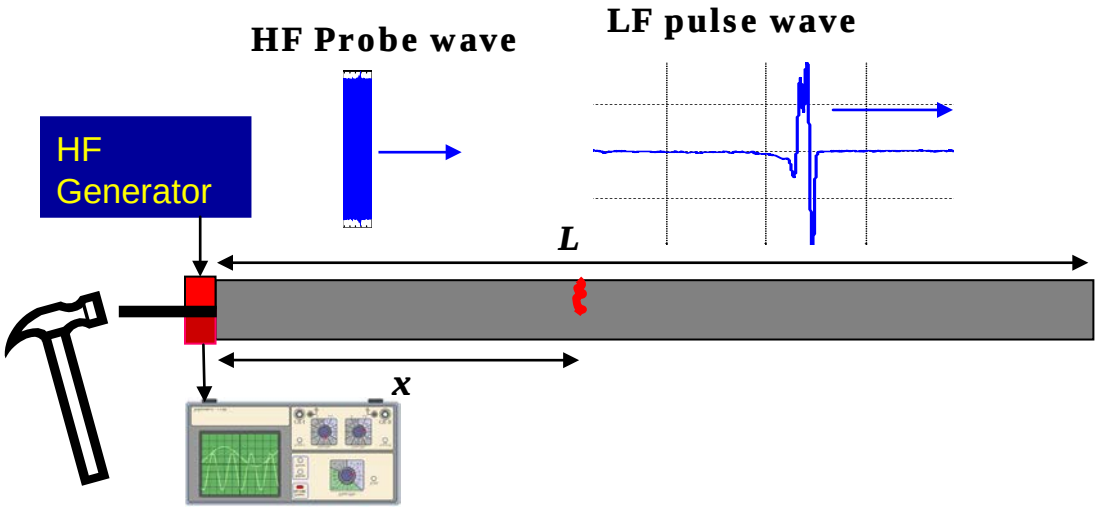

In this configuration, the HF probe wave interacts with the LF probe wave reflected from the other side of the rod. These waves meet at distance (x) if the time delay satisfies the condition

$$\frac{2L - x}{V_{im}} = \tau + \frac{x}{V_{hf}} \tag{3}$$

A.3.2 Experiment setup

The main part of the experiment was conducted according to the following setup as shown in Figure 45.

Figure 45. Schema of the experimental setup for measurements of the interaction of the HF tone burst signal with impact-produced acoustic impulse.

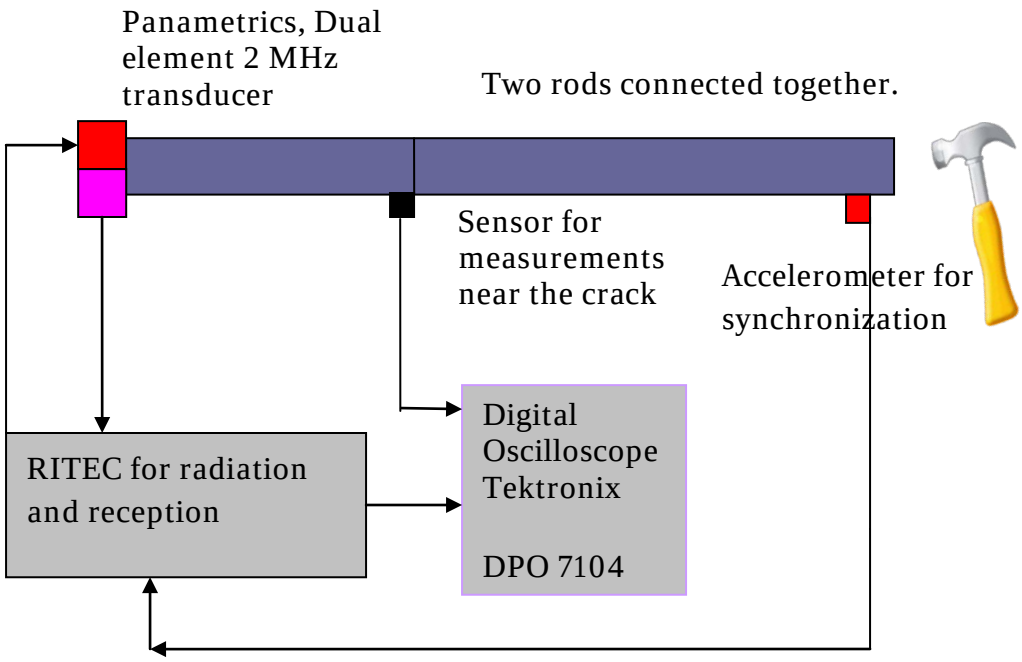

The tested trunnion rod has a diameter of 31.75 mm. The crack imitation was presented by contact of two rods having lengths of 6.07 m and 9.2 m. Both rods were connected together using clamps as shown in Figure 46.

Figure 46. The contact between two rods imitating the crack.

The radiation and reception of the HF tone burst signal were conducted by dual element sensor Panametrics Olympus 2.25 MHz. The tone burst signal was produced by a RITEC SNAP System (http://www.ritecinc.com/snapspecs.pdf), and the gated amplifier of the Ritec system was used for the signal reception. The small accelerometer attached to the right side of the rod was used for the system synchronization. The radiation of the HF pulse was conducted

with a time delay (after the hammer impact. The variability of this time delay allows changing of the area of the pulses' interaction.

The important consideration is choosing the frequency of the probe wave. This wave has to propagate through the whole rod and return without significant attenuation. The problem of ultrasonic wave application to an inspection of imbedded structures was investigated for many years (Pavalakovic et al. 2001; Beard et al 2003). The main goal of the work (Beard et al. 2003) was finding the modes that can propagate along the solid rod without leaking the energy to the surroundings. In this case, low attenuation allows application of the use of ultrasound for the inspection of structural elements at long distances. Investigations of ultrasound propagation in steel rod embedded in cement grout demonstrated that HF modes can propagate with low attenuation and have a group speed approximating the sound of longitudinal waves in infinite media. The previous experiments conducted at ERDC (Evans et al. 2013; Evans and Haskins 2013a,b) demonstrated that these nonleaky waves have a frequency of approximately 2 MHz; this frequency was used for the excitation of the HF wave probe in the test. Specifically, 2.048 MHz was used for the HF signal with the duration varying from 60 to 400 cycles. The separation of the HF and LF received signal was done in MatLab during signal processing using band pass filtering. The received signals were filtered in the LF band (2–200 kHz) for the measurements of the hammer-induced LF signal and in the HF band (1.8–2.2 MHz) for the measurements of the HF wave.

A.3.3 Test results

For calculation of the time delay required for the interaction of the HF wave and the mechanical impulses on the crack, the time delay of wave propagation and speed of the mechanical pulse and the HF pulse were estimated. This estimation was conducted for the case when the time delay (t) between the hammer impulse and the radiation of HF tone burst wave was 1.4 msec., and the pulses did not interact in the imitated crack. The HF burst contained 400 cycles of the ultrasonic wave, and its duration was approximately 0.2 msec. Figure 47 shows an example of the recorded signal when the sequence of the mechanical LF pulses (red) and the HF pulses (blue) is presented. This sequence is produced by reflection of pulses from the left end of the rod and the imitated crack. The distance between them is L_1 = 6.07 m, and the wave speed can be calculated as $V = 2L_1/T$, where T is the repetition time between the observed pulses.

Figure 47. The example of the recorded signal when the sequence of the mechanical pulses (red) and the HF pulses (blue) is presented in the plot above.

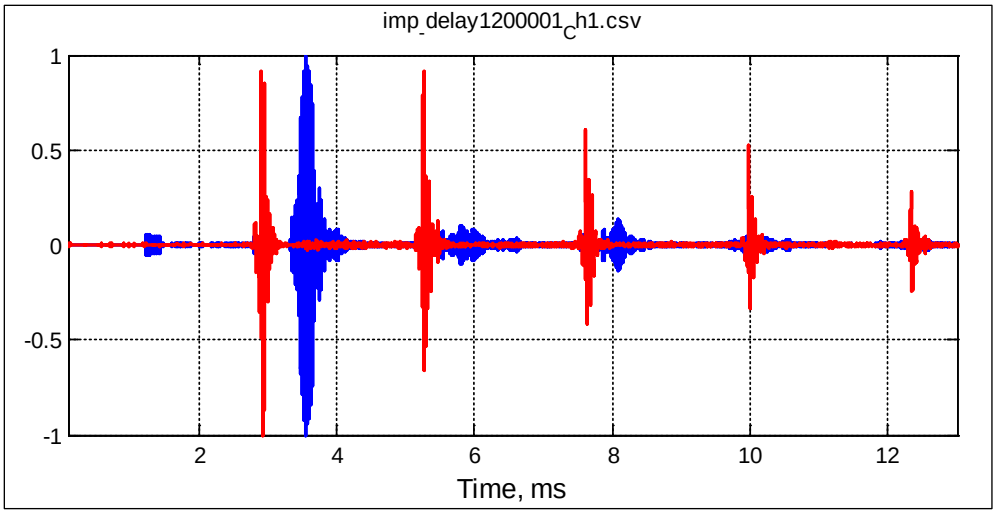

In Figure 47, the time interval between the mechanically produced pulses is 2.36 msec, and the time interval between the HF pulses is 2.12 msec. The estimation of the speed propagation from this time interval gives

$$V_{hf} = 5755 m/s, \qquad V_{im} = 5140 m/s \tag{4}$$

It is seen that the speed for the HF probe wave is close to the velocity of the longitudinal wave in bulk material and the speed of the impulse wave is slightly faster than the velocity of longitudinal wave (extensional wave in thin rods). The variation of the time delay (τ) between the mechanical impact and the HF wave allows both waves to interact at the simulated crack's position. Figure 47 shows the LF mechanical impulse recorded by sensor near the crack and the HF pulse at the same point. The sensor near the crack had limited frequency bandwidth and could not record the HF pulse. The HF pulse shown in Figure 48 is the HF pulse recorded by the Panametrics sensor near the left end of the rod and shifted in time to a half-of-time between radiation of the HF pulse and its reception. The time delay (τ) was 0.54 msec, and in this case, the part of the HF pulse interacted with the LF mechanical pulse.

Figure 48. The LF mechanical impulse recorded by sensor near the crack (red) and the HF pulse at the same point (blue) for the time delay τ= 0.54 msec.

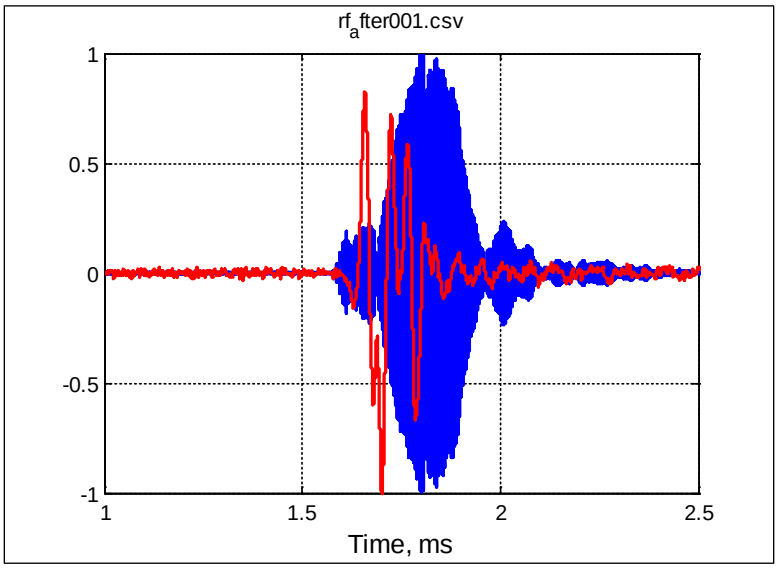

Figure 49 shows the signals received by the Panametrics sensor on the right side. It indicates that the beginning of the HF pulse had less amplitude than the second part of the pulse. This means that the interaction of the HF pulse with the LF mechanical pulse led to the increasing of the HF pulse amplitude while that portion of the pulse that does not interact remains unchanged.

Figure 49. The LF mechanical impulse recorded by the Panametrics sensor (red) and the HF pulse reflected from the simulated crack (blue) for the time delay τ= 0.54 msec.

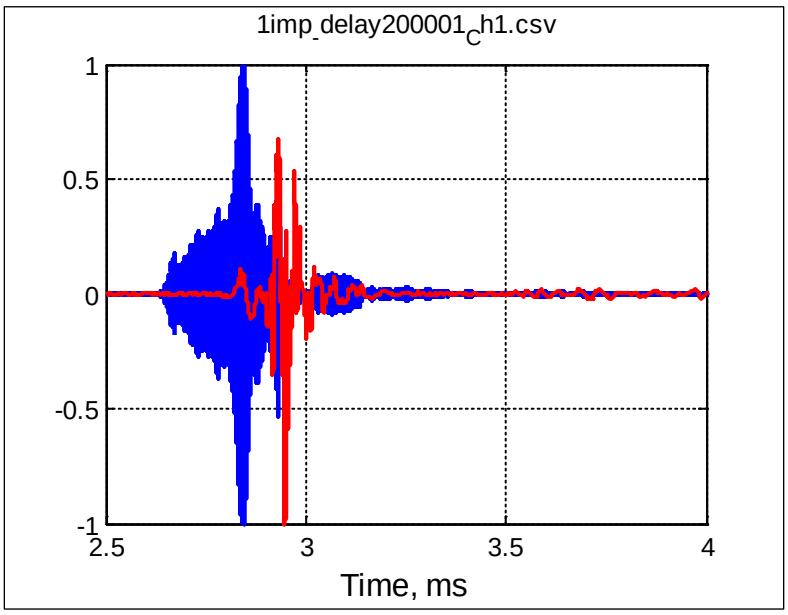

The increasing of the HF signal reflected from a simulated crack in the time of interaction with the LF mechanical wave can be explained by increasing the average contact area under the action of the mechanical pulse. The increasing of contact area led to increasing of the energy of the wave passing through the crack and decreasing of the wave reflected from the crack.

The variation of the time delay (τ) between the two pulses moved the area of the interaction from the crack, and in this case, the interaction between the two signals became practically invisible. Figure 50 shows the received pulses for the time delay τ = 1.4 msec. In this case, the LF mechanical pulse does have an influence on the form of the HF tone burst wave.

Figure 50. The LF mechanical impulse recorded by the Panametrics sensor (red) and the HF pulse reflected from the simulated crack (blue) for the time delay τ =1.4 ms. There is no interaction between these pulses.

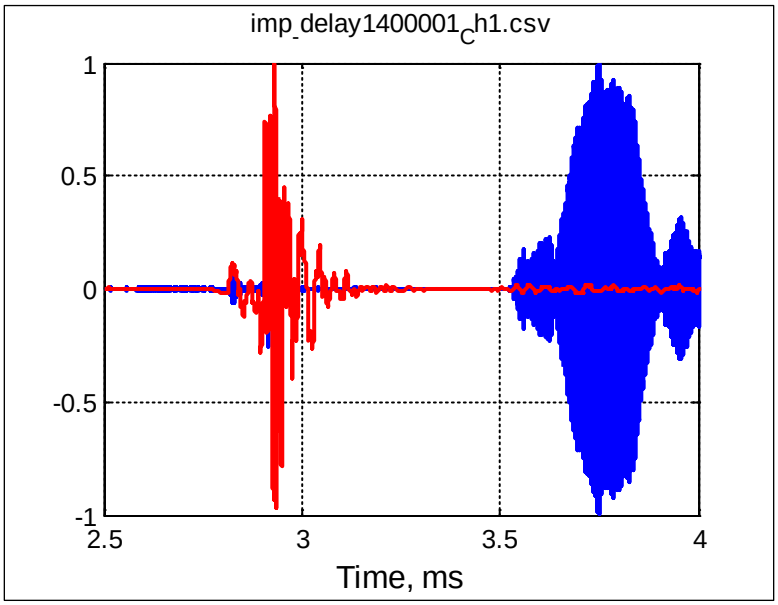

A.4 Conclusion

There was an investigation of the interaction of an ultrasonic tone burst wave with LF pulse produced by the hammer impact in a long trunnion rod. The HF (2MHz) tone burst emitter produced the higher-order longitudinal guided wave having low attenuation in the trunnion rods. The pulse interaction took place when both pulses met at the crack. Variation of the time delay between impulse radiations allows changing of the interaction area and can be used for crack localization. The investigated

effect can be basis for the new method of the nonlinear acoustic NDE that will be extremely sensitive to the presence of closed (kissing) cracks that cannot be detected by other methods.

Verification is planned of the tested method for various kinds of cracks in free trunnion rods and for the trunnion rods inside steel pipe filled by grease that is typical for anchor spillway gates.

REPORT DOCUMENTATION PAGE

Form Approved
OMB No. 0704-0188

1. REPORT DATE	2. REPORT TYPE	3. DATES COVERED *(From - To)*
July 2015	**Technical Report**	**1 Oct 13–30 Sept 14**

4. TITLE AND SUBTITLE
Detection of Microcracks in Trunnion Rods Using Ultrasonic Guided Waves

5a. CONTRACT NUMBER

5b. GRANT NUMBER

5c. PROGRAM ELEMENT NUMBER

6. AUTHOR(S)
James A. Evans and Rick Haskins

5d. PROJECT NUMBER

5e. TASK NUMBER

5f. WORK UNIT NUMBER

7. PERFORMING ORGANIZATION NAME(S) AND ADDRESS(ES)
Information Technology Laboratory
U.S. Army Engineer Research and Development Center
3909 Halls Ferry Road
Vicksburg, MS 39180-6199

8. PERFORMING ORGANIZATION REPORT NUMBER
ERDC/ITL TR-15-1

9. SPONSORING/MONITORING AGENCY NAME(S) AND ADDRESS(ES)
Navigational Research Program
Coastal Hydraulics Laboratory (CHL)

10. SPONSOR/MONITOR'S ACRONYM(S)

11. SPONSOR/MONITOR'S REPORT NUMBER(S)

12. DISTRIBUTION/AVAILABILITY STATEMENT
Approved for public release; distribution is unlimited.

13. SUPPLEMENTARY NOTES

14. ABSTRACT

Posttensioned rods are used to anchor spillway gates and transfer the forces from the reservoir pool through the gates to the spillway structures. Large tensile loads are applied to these high-strength steel rods to compress the surrounding concrete and prevent it from experiencing excessive destructive tensile forces. These rods are now experiencing ongoing failures. The Corps of Engineers is in need of reliable nondestructive testing (NDT) methods that are rapid, robust, and capable of detecting and quantifying defects.

Methods to detect microcracks are required to be rapid because of the large number of rods that exist at some installations. Robustness is required to handle the significant variations in design, construction, and field conditions that are known to exist. Defect detection and quantification provides tracking and monitoring data important for planning and prioritizing remediation efforts or operational practices.

This research to date has defined and demonstrated acoustical guided waves as a methodology to detect cracks that are orthogonal to the axis of the trunnion rods. A test method and equipment specifications have been developed as well as methods for dealing with field conditions such as anchor rods with rough cut ends.

15. SUBJECT TERMS		
Greenup Lock and Dam	Microcracks	Trunnion rods
Guided waves	Nondestructive testing	
	Posttensioned rods	

16. SECURITY CLASSIFICATION OF:			17. LIMITATION OF ABSTRACT	18. NUMBER OF PAGES	19a. NAME OF RESPONSIBLE PERSON
a. REPORT	b. ABSTRACT	c. THIS PAGE			**James A. Evans**
Unlimited	**Unlimited**	**Unlimited**	**SAR**	75	**19b. TELEPHONE NUMBER** *(Include area code)* **601-634-2535**